Zeitschrift: Cahiers d'archéologie romande
Herausgeber: Bibliothèque Historique Vaudoise
Band: 168 (2018)

Artikel: Tolochenaz (VD) - La Caroline : du mésolithique à l'époque romaine en passant par la nécropole du Boiron
Autor: Gallay, Audrey / Burri-Wyser, Elena / Menna, François
Anhang: Annexes
Autor: [s.n.]
DOI: https://doi.org/10.5169/seals-1036606

ANNEXES

ANNEXE 1 Tableau synthétique présentant, par période, les différents types de structures représentés et le nombre de structures concernées.

Attribution	Nb de structures	Pourcentage par période	Inhumation	Liée au rite funéraire de la crémation	Fossé	Foyer en cuvette à pierres chauffées	Foyer en fosse ou rejet	Fosse de combustion	Fosse à fonction indéterminée
Mésolithique	1	1 %						1	
Néolithique moyen	38	22 %	1	1		31	3	1	1
Bronze récent	2	1 %				2			
Bronze final	23	13 %	17	1	3	1	1		
La Tène	2	1 %		2					
Epoque romaine	28	16 %	1	15			6	5	1
Datation indéterminée	80	46 %		1		43	36		

Nb total de structures	174	Nb de structures	19	20	3	77	46	7	2
		Pourcentage par type de structure	11 %	11 %	2 %	44 %	26 %	4 %	< 1 %

ANNEXE 2 Inventaire des structures présenté par numéros croissants avec attributions typologique et chronologique. La dernière colonne indique le numéro d'inventaire du mobilier.

Structure	Type	Chronologie	Inv. mobilier
1002	fossé	Bronze final	26612
1018	sépulture à inhumation	Bronze final	26634
1030	sépulture à inhumation	Bronze final	26613
1052	sépulture à inhumation	Bronze final	26632 et 26635
1053	liée au rite funéraire de la crémation	Epoque romaine	26628
1057	sépulture à inhumation	Bronze final	26637
1058	liée au rite funéraire de la crémation	Epoque romaine	26648
1059	sépulture à inhumation	Bronze final	26615
1061	sépulture à inhumation	Bronze final	26636
1063	liée au rite funéraire de la crémation	Epoque romaine	26618
1064	liée au rite funéraire de la crémation	Epoque romaine	26617
1065	liée au rite funéraire de la crémation	Epoque romaine	26619
1066	liée au rite funéraire de la crémation	Epoque romaine	26622
1067	liée au rite funéraire de la crémation	Epoque romaine	26620
1069	sépulture à inhumation	Bronze final	26616
1070	sépulture à inhumation	Bronze final	26639
1071	sépulture à inhumation	Bronze final	26638
1073	sépulture à inhumation	Epoque romaine	26643
1074	sépulture à inhumation	Bronze final	26631
1075	liée au rite funéraire de la crémation	Epoque romaine	26623
1076	foyer en fosse ou rejet	Epoque romaine	26626
1077	sépulture à inhumation	Bronze final	26629
1079	sépulture à inhumation	Bronze final	26627
1080	sépulture à inhumation	Bronze final	26633
1083	sépulture à inhumation	Bronze final	26630
1084	sépulture à inhumation	Bronze final	26642
1085	fossé	Bronze final	-
1086	sépulture à inhumation	Bronze final	26650
1088	fossé	Bronze final	26667
1089	liée au rite funéraire de la crémation	Bronze final	26624
1090	sépulture à inhumation	Néolithique moyen	26625
1093	liée au rite funéraire de la crémation	Epoque romaine	26640
1094	liée au rite funéraire de la crémation	Epoque romaine	26644
1095	liée au rite funéraire de la crémation	Epoque romaine	26645
1096	liée au rite funéraire de la crémation	Epoque romaine	26651
1098	liée au rite funéraire de la crémation	Epoque romaine	26656
1103	liée au rite funéraire de la crémation	Epoque romaine	26649
1104	foyer en fosse ou rejet	Non daté: Protohistoire	26652
1105	foyer en cuvette à pierres chauffées	Non daté	-
1107	fosse à fonction indéterminée	Epoque romaine	26647
1111	sépulture à inhumation	Bronze final	26653
1114	foyer en cuvette à pierres chauffées	Non daté: Implanté dans un fossé Bronze final (St. 1002)	-

Structure	Type	Chronologie	Inv. mobilier
1115	liée au rite funéraire de la crémation	Non daté : Implanté dans un fossé Bronze final (St. 1002)	26658
1116	foyer en cuvette à pierres chauffées	Néolithique moyen	26661
1117	foyer en cuvette à pierres chauffées	Non daté	-
1118	foyer en cuvette à pierres chauffées	Non daté	St118
2001	foyer en cuvette à pierres chauffées	Non daté	-
2002	foyer en cuvette à pierres chauffées	Néolithique moyen	St2
2003	foyer en fosse ou rejet	Non daté	-
2004	foyer en fosse ou rejet	Non daté	-
2005	foyer en cuvette à pierres chauffées	Non daté	St5
2006	foyer en cuvette à pierres chauffées	Bronze final	-
2007	foyer en fosse ou rejet	Non daté	-
2008	foyer en cuvette à pierres chauffées	Néolithique moyen	-
2010	foyer en fosse ou rejet	Non daté	St10
2011	foyer en cuvette à pierres chauffées	Non daté	-
2012	foyer en cuvette à pierres chauffées	Non daté	St12
2013	foyer en fosse ou rejet	Non daté	-
2014	liée au rite funéraire de la crémation	La Tène	St14
2015	foyer en cuvette à pierres chauffées	Non daté	St15
2016	foyer en fosse ou rejet	Non daté	St16
2017	fosse de combustion	Epoque romaine	-
2018	foyer en cuvette à pierres chauffées	Non daté	-
2019	foyer en cuvette à pierres chauffées	Non daté	St19
2020	foyer en cuvette à pierres chauffées	Non daté	St20
2021	foyer en fosse ou rejet	Non daté	-
2022	liée au rite funéraire de la crémation	La Tène	St22
2023	foyer en cuvette à pierres chauffées	Non daté	-
2024	foyer en fosse ou rejet	Non daté	St24
2025a	foyer en fosse ou rejet	Non daté	-
2025b	foyer en cuvette à pierres chauffées	Non daté	-
2026	foyer en cuvette à pierres chauffées	Bronze récent	St26
2028	foyer en cuvette à pierres chauffées	Non daté	-
2029	foyer en cuvette à pierres chauffées	Non daté	-
2032	foyer en fosse ou rejet	Epoque romaine	St32
2033	foyer en fosse ou rejet	Epoque romaine	-
2036	fosse de combustion	Epoque romaine	St36
2037	foyer en cuvette à pierres chauffées	Néolithique moyen	St37
2038	fosse de combustion	Epoque romaine	St38
2039	fosse de combustion	Néolithique moyen	St39
2040	foyer en cuvette à pierres chauffées	Non daté	-
2042	foyer en fosse ou rejet	Epoque romaine	-
2043	foyer en fosse ou rejet	Néolithique moyen	St43
2044	fosse de combustion	Mésolithique	St44
2045	foyer en cuvette à pierres chauffées	Non daté	-
2046	foyer en cuvette à pierres chauffées	Non daté	-
2047	foyer en cuvette à pierres chauffées	Non daté	-
2048	foyer en cuvette à pierres chauffées	Non daté	-

Structure	Type	Chronologie	Inv. mobilier
2050	foyer en fosse ou rejet	Non daté	-
2051	foyer en cuvette à pierres chauffées	Néolithique moyen	-
2052	foyer en cuvette à pierres chauffées	Néolithique moyen	St52
2053	foyer en fosse ou rejet	Non daté	St53
2057	foyer en fosse ou rejet	Non daté	-
2058	foyer en fosse ou rejet	Non daté	-
2059	foyer en cuvette à pierres chauffées	Néolithique moyen	St59
2060	foyer en fosse ou rejet	Néolithique moyen	St60
2061	foyer en fosse ou rejet	Non daté	-
2063	foyer en cuvette à pierres chauffées	Néolithique moyen	St63
2065	foyer en fosse ou rejet	Non daté	-
2068	foyer en cuvette à pierres chauffées	Néolithique moyen	St68
2069	foyer en cuvette à pierres chauffées	Non daté	-
2070	foyer en fosse ou rejet	Non daté	-
2071	foyer en fosse ou rejet	Non daté	-
2072	foyer en fosse ou rejet	Non daté	-
2075	foyer en fosse ou rejet	Bronze final	-
2076	foyer en fosse ou rejet	Non daté	-
2077	foyer en cuvette à pierres chauffées	Non daté	-
2078	foyer en cuvette à pierres chauffées	Bronze récent	27931
2079	foyer en fosse ou rejet	Non daté	27821
2080	foyer en cuvette à pierres chauffées	Non daté	-
2081	foyer en cuvette à pierres chauffées	Néolithique moyen	27914
2082	foyer en cuvette à pierres chauffées	Non daté	-
2084	foyer en fosse ou rejet	Non daté	-
2085	fosse de combustion	Epoque romaine	27917
2086	foyer en cuvette à pierres chauffées	Non daté	-
2087	foyer en cuvette à pierres chauffées	Néolithique moyen	27850
2088	foyer en fosse ou rejet	Non daté	-
2089	foyer en cuvette à pierres chauffées	Non daté	-
2090	foyer en cuvette à pierres chauffées	Néolithique moyen	27822 et 27921
2091	fosse à fonction indéterminée	Néolithique moyen	27912
2093	foyer en cuvette à pierres chauffées	Néolithique moyen	27913
2094	foyer en fosse ou rejet	Non daté	-
2095	foyer en fosse ou rejet	Non daté	-
2096	foyer en fosse ou rejet	Non daté	-
2097	foyer en cuvette à pierres chauffées	Néolithique moyen	27943
2098	foyer en fosse ou rejet	Non daté	27824
2100	foyer en cuvette à pierres chauffées	Non daté	-
2101	liée au rite funéraire de la crémation	Epoque romaine	27925
2102	foyer en cuvette à pierres chauffées	Néolithique moyen	27928
2105	foyer en cuvette à pierres chauffées	Néolithique moyen	27826
2107	foyer en cuvette à pierres chauffées	Néolithique moyen	27936
2110	foyer en cuvette à pierres chauffées	Non daté	-
2113	foyer en fosse ou rejet	Epoque romaine	-
2114	foyer en fosse ou rejet	Non daté	-

Structure	Type	Chronologie	Inv. mobilier
2115	foyer en cuvette à pierres chauffées	Néolithique moyen	27937
2116	foyer en fosse ou rejet	Non daté	-
2117	foyer en cuvette à pierres chauffées	Non daté	-
2118	foyer en cuvette à pierres chauffées	Néolithique moyen	27804 et 27815 à 27818
2119	foyer en fosse ou rejet	Non daté	-
2120	foyer en cuvette à pierres chauffées	Néolithique moyen	27945
2121	foyer en cuvette à pierres chauffées	Non daté	-
2122	foyer en cuvette à pierres chauffées	Non daté	-
2123	foyer en cuvette à pierres chauffées	Néolithique moyen	27807
2124	foyer en cuvette à pierres chauffées	Non daté	27829 et 27830
2125	foyer en cuvette à pierres chauffées	Non daté	27940
2126	foyer en cuvette à pierres chauffées	Néolithique moyen	27950
2127	foyer en cuvette à pierres chauffées	Néolithique moyen	27801
2129	foyer en cuvette à pierres chauffées	Néolithique moyen	27946
2130	liée au rite funéraire de la crémation	Néolithique moyen	27806
2131	foyer en cuvette à pierres chauffées	Néolithique moyen	27810 et 27831
2134	foyer en cuvette à pierres chauffées	Néolithique moyen	27996
2135	foyer en cuvette à pierres chauffées	Non daté	27832
2136	foyer en fosse ou rejet	Non daté	-
2137	foyer en cuvette à pierres chauffées	Néolithique moyen	27805
2138	foyer en fosse ou rejet	Epoque romaine	-
2139	foyer en cuvette à pierres chauffées	Non daté	-
2140	foyer en cuvette à pierres chauffées	Non daté	-
2141	foyer en fosse ou rejet	Non daté	-
2142	foyer en fosse ou rejet	Néolithique moyen	27834
2143	foyer en cuvette à pierres chauffées	Non daté	-
2144	foyer en fosse ou rejet	Non daté	-
2145	foyer en cuvette à pierres chauffées	Néolithique moyen	27803
2146	foyer en cuvette à pierres chauffées	Néolithique moyen	27949
2149	foyer en cuvette à pierres chauffées	Non daté	-
2151	foyer en fosse ou rejet	Non daté	-
2152	foyer en cuvette à pierres chauffées	Néolithique moyen	27835, 27836 et 27947
2153	foyer en cuvette à pierres chauffées	Non daté	-
2155	foyer en cuvette à pierres chauffées	Néolithique moyen	27819 et 27924
2156	fosse de combustion	Epoque romaine	27923
2157	foyer en fosse ou rejet	Non daté	-
2158	foyer en cuvette à pierres chauffées	Non daté	-
2159	foyer en fosse ou rejet	Non daté	-
2160	foyer en cuvette à pierres chauffées	Non daté	-
2161	foyer en cuvette à pierres chauffées	Non daté	-

ANNEXE 3 Catégories de mobilier par structure, présenté par numéros d'inventaire du mobilier croissants; avec numéros de structures, attributions chronologiques, et types de mobilier présents dans chaque ensemble. La dernière colonne indique les éventuels éléments typochronologiquement intrusifs. Les structures auxquelles ont été attribués plusieurs numéros d'inventaire de mobilier figurent en italique.

Inv. mobilier	Structure	Chronologie	Céramique	Bronze	Fer	Verre	Silex	Lithique autre	Os brûlé	Os humain non brûlé	Nodules de charbon	Autres	Eléments intrusifs
26612	1002	Bronze final	x										
26613	1030	Bronze final	x										
26615	1059	Bronze final	x	x						x			
26616	1069	Bronze final	x							x			
26617	1064	Epoque romaine	x		x	x			x			rondelle en os	
26618	1063	Epoque romaine	x		x	x	x		x				
26619	1065	Epoque romaine	x		x				x				
26620	1067	Epoque romaine	x		x	x			x				1 tesson de céramique protohistorique
26621	mobilier hors contexte	Epoque romaine	x			x							
26622	1066	Epoque romaine	x		x				x		x		
26623	1075	Epoque romaine	x		x	x			x		x		
26624	1089	Bronze final	x	x		x			x				
26625	1090	Néolithique moyen								x		perles en lignite	
26626	1076	Epoque romaine	x									échantillon carpologique	
26627	1079	Bronze final	x	x				x					
26628	1053	Epoque romaine	x	x	x				x		x	figurine en terre cuite	
26629	1077	Bronze final	x	x				x					
26630	1083	Bronze final		x						x			
26631	1074	Bronze final	x	x				x		x			
26632	1052	Bronze final	x										
26633	1080	Bronze final	x							x			
26634	1018	Bronze final	x	x						x		perles en ambre	
26635	1052	Bronze final	x	x						x			
26636	1061	Bronze final		x		x		x		x		perles en faïence vitreuse et en ambre	

Inv. mobilier	Structure	Chronologie	Céramique	Bronze	Fer	Verre	Silex	Lithique autre	Os brûlé	Os humain non brûlé	Nodules de charbon	Autres	Eléments intrusifs
26637	1057	Bronze final								x			
26638	1071	Bronze final	x							x			
26639	1070	Bronze final		x						x			
26640	1093	Epoque romaine	x		x				x		x		
26641	mobilier hors contexte	Epoque romaine	x										
26642	1084	Bronze final										perles en ambre	
26643	1073	Epoque romaine	x	x						x		2 monnaies	
26644	1094	Epoque romaine	x		x				x				
26645	1095	Epoque romaine	x		x	x			x		x		
26646	mobilier hors contexte	Epoque romaine	x		x							rondelle en os, TCA	
26647	1107	Epoque romaine	x								x		
26648	1058	Epoque romaine		x	x				x		x		Verre moderne
26649	1103	Epoque romaine	x	x	x	x			x				
26650	1086	Bronze final								x		perle en ambre	
26651	1096	Epoque romaine	x		x				x			perle en lignite	
26652	1104	Non daté: Protohistoire	x										
26653	1111	Bronze final	x	x						x			
26656	1098	Epoque romaine				x			x				
26657	mobilier hors contexte	Epoque romaine	x										
26658	1115	Non daté: implanté dans un fossé Bronze final (St. 1002)							x				
26661	1116	Néolithique moyen	x										
26667	1088	Bronze final							x				Céramique et fer d'époque romaine

Inv. mobilier	Structure	Chronologie	Céramique	Bronze	Fer	Verre	Silex	Lithique autre	Os brûlé	Os humain non brûlé	Nodules de charbon	Autres	Eléments intrusifs
26668	mobilier hors contexte	Epoque romaine	x										
27801	2127	Néolithique moyen						x					
27803	2145	Néolithique moyen	x				x	x					
27804	2118	Néolithique moyen	x				x	x					
27805	2137	Néolithique moyen	x				x						
27806	2130	Néolithique moyen	x				x	x	x				
27807	2123	Néolithique moyen	x				x	x					
27808	mobilier hors contexte	Néolithique moyen						x					
27810	2131	Néolithique moyen	x					x					
27815	2118	Néolithique moyen	x					x					
27816	2118	Néolithique moyen	x										
27817	2118	Néolithique moyen	x										
27818	2118	Néolithique moyen						x					
27819	2155	Néolithique moyen	x				x						
27821	2079	Non daté									x		
27822	2090	Néolithique moyen						x					
27824	2098	Non daté									x		
27826	2105	Néolithique moyen					x						
27829	2124	Non daté									x		
27830	2124	Non daté									x		
27831	2131	Néolithique moyen	x										
27832	2135	Non daté									x		
27834	2142	Néolithique moyen					x						
27835	2152	Néolithique moyen	x				x	x					
27836	2152	Néolithique moyen					x						
27850	2087	Néolithique moyen	x										
27912	2091	Néolithique moyen					x						
27913	2093	Néolithique moyen						x					
27914	2081	Néolithique moyen					x						

Inv. mobilier	Structure	Chronologie	Céramique	Bronze	Fer	Verre	Silex	Lithique autre	Os brûlé	Os humain non brûlé	Nodules de charbon	Autres	Eléments intrusifs
27915	Couche	Néolithique moyen					x						
27917	2085	Epoque romaine											2 tessons de céramique moderne
27921	2090	Néolithique moyen						x					
27923	2156	Epoque romaine										TCA	
27924	2155	Néolithique moyen					x						
27925	2101	Epoque romaine	x	x	x	x			x		x		1 tesson de céramique protohistorique
27928	2102	Néolithique moyen						x					
27931	2078	Bronze récent									x		
27936	2107	Néolithique moyen	x										
27937	2115	Néolithique moyen						x					
27940	2125	Non daté									x		
27943	2097	Néolithique moyen						x					
27945	2120	Néolithique moyen					x						
27946	2129	Néolithique moyen	x					x					
27947	2152	Néolithique moyen	x				x	x					
27948	Couche	Néolithique moyen	x										
27949	2146	Néolithique moyen	x					x					
27950	2126	Néolithique moyen	x				x						
27996	2134	Néolithique moyen					x						
St2	2002	Néolithique moyen	x										
St5	2005	Non daté									x		
St10	2010	Non daté									x		
St12	2012	Non daté									x		
St14	2014	La Tène		x	x				x				
St15	2015	Non daté									x		
St16	2016	Non daté									x		
St19	2019	Non daté									x		
St20	2020	Non daté									x		

Inv. mobilier	Structure	Chronologie	Céramique	Bronze	Fer	Verre	Silex	Lithique autre	Os brûlé	Os humain non brûlé	Nodules de charbon	Autres	Eléments intrusifs
St22	2022	La Tène		x	x				x				
St24	2024	Non daté									x		
St26	2026	Bronze récent	x										
St32	2032	Epoque romaine										TCA	
St36	2036	Epoque romaine	x									TCA	
St37	2037	Néolithique moyen	x										
St38	2038	Epoque romaine											2 tessons de céramique protohistorique
St39	2039	Néolithique moyen	x				x						
St43	2043	Néolithique moyen	x										
St44	2044	Mésolithique					x						
St52	2052	Néolithique moyen	x					x					
St53	2053	Non daté									x		
St59	2059	Néolithique moyen	x				x						
St60	2060	Néolithique moyen	x										
St63	2063	Néolithique moyen	x										
St68	2068	Néolithique moyen	x					x					
St118	1118	Non daté									x		
vrac général	Secteur sud-ouest	Epoque romaine			x								

ANNEXE 4 Catalogue synthétique des inhumations. Toutes sont des sépultures primaires individuelles.

Structure	Attribution chronologique	Orientation (tête/pieds)	Plan	Dimensions [L x l x p en cm]	Organisation interne : éléments en matériau périssable	Dalles (oui / non)	Ostéologie	Mobilier : types d'objets représentés	Inv. mobilier	Chronologie
1073	Epoque romaine	NNO/SSE	rectangulaire, légèrement trapézoïdale	190 x 60 à 70 x 17		non	adulte, jeune ou mature, de sexe masculin	fibule, monnaies, tesson de céramique résiduel	26643	seconde moitié 1er siècle ap. J.-C.
1090	Néolithique moyen	ENE/OSO	rectangulaire	210 x 130 x 24	limites sédimentaires internes rectilignes	non	adulte, jeune ou mature	perles	26635	4452 - 4349 BC
1018	Bronze final	SOO/NEE	rectangulaire	> 150 x 90 x 37		oui	immature, âgé de 7.5 ans +/- 1.5 an	bracelet, épingle, perle, récipient	26634	HaB2-B3 ancien
1030	Bronze final	SOO/NEE	rectangulaire?	? x 70 x 50		non	aucun ossement conservé	récipient	26613	HaB3 récent
1052	Bronze final	SOO/NEE	rectangulaire	215 x 60 x 39	limites sédimentaires internes rectilignes	oui	adulte, âgé, de sexe masculin	rasoir, épingle, anneau, récipient	26632 et 26635	HaB3 ancien
1057	Bronze final	O/E	rectangulaire	190 x 80 x 34		oui	immature, âgé d'entre 12 et 15 ans		26637	HaB
1059	Bronze final	SOO/NEE	allongée	140 x 55 x 25	pierres de calage en fond de fosse	oui	immature, âgé de 4 ans +/- 1 an	bracelet, récipient	26615	HaB3
1061	Bronze final	SOO/NEE	rectangulaire	280 x 70 x 37		oui	adulte, mature, de sexe féminin	bracelet, anneaux de cheville, alêne, bagues, perles	26636	HaB1
1069	Bronze final	O/E	indéterminée	> 106 x 67 x 4		oui	grand adolescent ou adulte	récipient	26616	HaB3
1070	Bronze final	SOO/NEE	rectangulaire	> 155 x 45 x 32	pierres de calage en fond de fosse	oui	immature de la classe d'âge des 5-9 ans	bracelet, épingle	26639	HaB
1071	Bronze final	SOO/NEE	rectangulaire	250 x 90 x 61	pierre de calage en fond de fosse	oui	adulte	récipient	26638	HaB3
1074	Bronze final	SO/NE	rectangulaire	330 x 160 x 42	limites sédimentaires internes rectilignes	oui	adulte, jeune ou mature	épingle, récipient	26631	HaB3 ancien
1077	Bronze final	NO/SE	rectangulaire	260 x 60 x 30	pierres de calage en fond de fosse	oui	aucun ossement conservé	épingle, récipient	26629	HaB3 ancien
1079	Bronze final	NOO/SEE	rectangulaire	260 x 90 x 40		oui	grand adolescent ou adulte	épingle, anneau, tesson de céramique résiduel	26627	HaB
1080	Bronze final	SO/NE	rectangulaire	200 x 80 x 37	pierres de calage en fond de fosse	oui	immature, âgé de 7 à 7.5 ans +/- 1.5 an	récipient	26633	HaB3 récent
1083	Bronze final	NOO/SEE	rectangulaire	> 200 x 80 x 37		oui	grand adolescent ou adulte	épingle	26630	HaB3
1084	Bronze final	SOO/NEE	rectangulaire	130 x 60 x 29	pierres de calage en fond de fosse	oui	aucun ossement conservé	perles	26642	HaB
1086	Bronze final	SOO/NEE	rectangulaire	120 x 70 x 21		oui	immature, âgé de 5 ans +/- 1 an	perle	26650	HaB
1111	Bronze final	O/E	allongée, implantée dans le fossé St. 1088 au profil en cuvette et d'une largeur de 45 cm	> 150 x 45 x 9		non	adulte, mature ou âgé, probablement de sexe masculin	rasoir, épingle, anneau, récipients	26653	HaB3 récent

ANNEXE 5

Catalogue synthétique des structures liées au rite funéraire de la crémation.

Structure	Attribution chronologique	Structure primaire / secondaire	Type	Plan	Dimensions [L × l × p en cm]
1053	Epoque romaine	secondaire	sépulture	rectangulaire	150 × 60 × 37
1058	Epoque romaine	secondaire	indét. en raison d'un pillage moderne	rectangulaire	80 × 50 × 20
1063	Epoque romaine	secondaire	sépulture	circulaire	70 × 50 × 22
1064	Epoque romaine	secondaire	probable sépulture	circulaire	65 × 65 × 23
1065	Epoque romaine	secondaire	probable sépulture	circulaire	70 × 60 × 14
1066	Epoque romaine	secondaire	structure non sépulcrale	circulaire	60 × 60 × 26
1067	Epoque romaine	secondaire	structure non sépulcrale	ovale	65 × 50 × 12
1075	Epoque romaine	secondaire	sépulture avec vase ossuaire	ovale	72 × 50 × 20
1089	Bronze final	secondaire	sépulture avec vase ossuaire	circulaire	65 × 65 × 20
1093	Epoque romaine	secondaire	structure non sépulcrale	circulaire	80 × 70 × 26
1094	Epoque romaine	secondaire	structure non sépulcrale	circulaire	42 × >32 × 12
1095	Epoque romaine	primaire	bûcher en fosse	indéterminée	> 150 × 200 × 42
1096	Epoque romaine	secondaire	structure non sépulcrale	ovale	80 × 40 × 16
1098	Epoque romaine	secondaire	probable sépulture	circulaire	60 × 60 × 7
1103	Epoque romaine	secondaire	sépulture	circulaire	110 × 110 × 21
1115	Non daté	secondaire	sépulture avec concentration d'ossement	?	?
2014	La Tène ancienne	secondaire	probable sépulture	circulaire	76 × 65 × 12
2022	La Tène ancienne	secondaire	probable sépulture	quadrangulaire	88 × 74 × 21
2101	Epoque romaine	secondaire	probable sépulture	ovale	120 × 58 × 23
2130	Néolithique moyen	secondaire	sépulture ?	ovale	70 × 65 × 25

Organisation interne	Poids total d'os brûlé [g]	Ostéologie	Catégories de mobilier brûlé	Catégories de mobilier non brûlé	Inv. mobilier	Chronologie
comblement homogène, formé de résidus de crémation	435	individu adulte	céramique, bronze, fer et terre cuite	fer	26628	seconde moitié 1er - début 2e siècle ap. J.-C.
comblement homogène, formé de résidus de crémation	3	individu de taille adulte	bronze et fer		26648	dès fin 1er siècle ap. J.-C.
comblement formé de résidus de crémation, avec couronne périphérique plus sableuse	281	individu de taille adulte	céramique, verre, fer et silex	fer	26618	milieu 1er siècle ap. J.-C.
stratification interne : argilo-sableux dans la partie inférieure, résidus de crémation dans la partie supérieure et couronne périphérique plus sableuse	63	individu de taille adulte	céramique, verre et fer	rondelle en os	26617	fin 1er - 3e siècle ap. J.-C.
comblement formé de résidus de crémation, avec couronne périphérique plus sableuse	61	individu de taille adulte	céramique et fer		26619	fin 1er - 3e siècle ap. J.-C.
comblement formé de résidus de crémation, avec couronne périphérique plus sableuse	73	individu de taille adulte	céramique et fer		26622	début 2e ? - 3e siècle ap. J.-C.
comblement homogène, formé de résidus de crémation	2		céramique, verre et fer	fer	26620	
comblement homogène, formé de résidus de crémation	38	individu de taille adulte	céramique, verre et fer	céramique (vase ossuaire) et verre (balsamaire)	26623	milieu 1er - 3e siècle ap. J.-C.
présence d'un coffre/coffrage en matériau périssable contenant les résidus de crémation. Vase ossuaire déposé sur ou dans le coffre	173	individu de taille adulte	verre et bronze	céramique (vase ossuaire)	26624	HaB2-B3 ancien
comblement homogène, formé de résidus de crémation	43	individu de taille adulte	céramique et fer		26640	dernier tiers 1er - milieu 2e siècle ap. J.-C.
comblement homogène, formé de résidus de crémation	21	individu de taille adulte	céramique et fer		26644	
stratification interne : résidus de crémation dans la partie inférieure et limon sableux avec nodules de terre rubéfiée dans la partie supérieure	47	individu de taille adulte	céramique, verre et fer	verre (aryballe)	26645	dernier tiers 1er - premier quart 2e siècle ap. J.-C.
comblement homogène, formé de résidus de crémation	3		céramique et lignite	fer	26651	dernier tiers 1er - premier quart 2e siècle ap. J.-C.
comblement homogène, formé de résidus de crémation	133	individu de taille adulte	verre		26656	
comblement formé de résidus de crémation, avec couronne périphérique plus sableuse	36	individu de taille adulte	céramique, verre, bronze, fer et faune	fer	26649	milieu 1er - milieu 2e siècle ap. J.-C.
?	123	individu adulte				
comblement homogène, formé de résidus de crémation	31	individu adulte	bronze et fer		St14	LTA1
comblement homogène, formé de résidus de crémation	20	individu adulte	bronze et fer		St22	LTA1
stratification interne : de bas en haut, limon sableux peu charbonneux, résidus de crémation et limon sableux peu charbonneux	32	individu de taille adulte	céramique, verre, bronze et fer		27925	Env. 60 - 100 ap. J.-C.
comblement homogène, formé de résidus de crémation	13	individu de taille adulte	céramique (?), silex et quartz	céramique (?)	27806	Cortaillod ancien

ANNEXE 6 Catalogue synthétique des fossés.

Structure	Attribution chronologique	Type	Longeur ou diamètre interne [m]	Largeur et profondeur max. [m]	Orientation	Inv. mobilier
1002	Bronze final	fossé rectiligne	> 45	3 × 0.75	SO/NE	26612
1085	Bronze final	fossé circulaire	8	0.5 × 0.2		
1088	Bronze final	fossé rectiligne	> 45	0.7 × 0.33	SOO/NEE à SO/NE	26667

ANNEXE 7 Catalogue synthétique des structures de combustion, présenté par type de structure.

Foyers en cuvette à pierres chauffées							
Structure	Attribution chronologique	Plan	Dimensions [L × l × p en cm]	Rubéfaction	Galets / blocs	Inv. mobilier	Datation $_{14}$C calibrée
1105	Non daté	circulaire	80 × 78 × 21		galets rubéfiés		
1114	Non daté : implanté dans un fossé Bronze final (St. 1002)	ovale	130 × 80 × 24		blocs rubéfiés		
1116	Néolithique moyen	rectangulaire	120 × 100 × 50		galets rubéfiés	26661	
1117	Non daté	circulaire	108 × 100 × 50		galets rubéfiés		
1118	Non daté	circulaire	100 × 100 × 20		galets rubéfiés	St118	
2001	Non daté	circulaire	60 × 50 × 12		galets rubéfiés		
2002	Néolithique moyen	rectangulaire	96 × 80 × 38	sédiment encaissant	galets rubéfiés	St2	4230 - 3987 BC
2005	Non daté	ovale	90 × 60 × 14		galets rubéfiés	St5	
2006	Bronze final	ovale	92 × 66 × 35		galets rubéfiés		980 - 820 BC
2008	Néolithique moyen	circulaire	120 × 114 × 46	comblement et sédiment encaissant	galets rubéfiés		3954 - 3789 BC
2011	Non daté	circulaire	110 × 108 × 40	sédiment encaissant	galets rubéfiés		
2012	Non daté	ovale	128 × 110 × 24	sédiment encaissant	galets rubéfiés	St12	
2015	Non daté	rectangulaire	96 × 90 × 16		galets rubéfiés	St15	
2018	Non daté	ovale	116 × 92 × 48	sédiment encaissant	galets rubéfiés		
2019	Non daté	carrée	82 × 74 × 23	sédiment encaissant	galets rubéfiés	St19	
2020	Non daté	rectangulaire	100 × 66 × 16		galets rubéfiés	St20	
2023	Non daté	rectangulaire	80 × 74 × 20		galets rubéfiés		
2025b	Non daté	rectangulaire?	80 ×? × 11		galets rubéfiés		
2026	Bronze récent	ovale	100 ×? × 32		galets rubéfiés	St26	
2028	Non daté	ovale	136 × 120 × 33	comblement et sédiment encaissant	galets rubéfiés		
2029	Non daté	circulaire	64 × 60 × 28	sédiment encaissant	galets rubéfiés		

Foyers en cuvette à pierres chauffées							
Structure	Attribution chronologique	Plan	Dimensions [L × l × p en cm]	Rubéfaction	Galets / blocs	Inv. mobilier	Datation $_{14}$C calibrée
2037	Néolithique moyen	carrée	88 × 88 × 19	sédiment encaissant	galets rubéfiés	St37	
2040	Non daté	rectangulaire	96 × 46 × 25		galets rubéfiés		
2045	Non daté	ovale	100 × 66 × 20		galets rubéfiés		
2046	Non daté	rectangulaire	88 × 64 × 16		galets rubéfiés		
2047	Non daté	rectangulaire	82 × 74 × 35	sédiment encaissant	galets rubéfiés		
2048	Non daté	ovale	96 × 74 × 24	sédiment encaissant	galets rubéfiés		
2051	Néolithique moyen	circulaire	98 × 90 × 33	sédiment encaissant	galets rubéfiés		4228 - 3981 BC
2052	Néolithique moyen	rectangulaire	98 × 88 × 48		galets rubéfiés	St52	
2059	Néolithique moyen	carrée?	94 × 84 × 26	sédiment encaissant	galets rubéfiés	St59	3966 - 3787 BC
2063	Néolithique moyen	carrée?	128 × 120 × 66	sédiment encaissant	galets rubéfiés	St63	
2068	Néolithique moyen	circulaire	140 × 130 × 48	sédiment encaissant	galets rubéfiés	St68	4231 - 3990 BC
2069	Non daté	ovale	86 × 70 × 13		galets rubéfiés		
2077	Non daté	rectangulaire	190 × 120 × 13		galets rubéfiés		
2078	Bronze récent	rectangulaire	255 × 130 × 13		blocs thermofractés	27931	1192 - 980 BC
2080	Non daté	circulaire	70 × 70 × 16		galets rubéfiés		
2081	Néolithique moyen	ovale	80 × 55 × 23		galets rubéfiés	27914	
2082	Non daté	rectangulaire	120 × 100 × 28		galets rubéfiés		
2086	Non daté	circulaire	75 × 75 × 16		galets rubéfiés		
2087	Néolithique moyen	circulaire	80 × 80 × 24		galets rubéfiés	27850	
2089	Non daté	circulaire	90 × 90 × 25		galets rubéfiés		
2090	Néolithique moyen	circulaire	74 × 74 × 25		galets rubéfiés	27822 et 27921	
2093	Néolithique moyen	carrée	105 × 105 × 18		galets rubéfiés	27913	
2097	Néolithique moyen	rectangulaire	110 × 100 × 28		galets rubéfiés	27943	
2100	Non daté	circulaire	65 × 65 × 17		galets rubéfiés		
2102	Néolithique moyen	carrée	100 × 100 × 5		blocs thermofractés	27928	
2105	Néolithique moyen	circulaire	80 × 80 × 25		galets rubéfiés	27826	
2107	Néolithique moyen	indét.	195 × 110 × 40	sédiment encaissant	galets rubéfiés	27936	
2110	Non daté	circulaire	70 × 70 × 10		galets rubéfiés		
2115	Néolithique moyen	circulaire	65 × 65 × 19		galets rubéfiés	27937	
2117	Non daté	ovale	90 × 60 × 26		galets rubéfiés		
2118	Néolithique moyen	circulaire	102 × 102 × 35		galets rubéfiés	27804 et 27815 à 27818	

Foyers en cuvette à pierres chauffées							
Structure	Attribution chronologique	Plan	Dimensions [L × l × p en cm]	Rubéfaction	Galets / blocs	Inv. mobilier	Datation ^{14}C calibrée
2120	Néolithique moyen	circulaire	95 × 95 × 34		galets rubéfiés	27945	
2121	Non daté	ovale	90 × 70 × 32		blocs et dallette		
2122	Non daté	circulaire	110 × 100 × 45	comblement	galets rubéfiés		
2123	Néolithique moyen	circulaire	75 × 75 × 32		galets rubéfiés	27807	
2124	Non daté	ovale	130 × 80 × 16		galets rubéfiés	27829 et 27830	
2125	Non daté	circulaire	70 × 60 × 16		galets rubéfiés	27940	
2126	Néolithique moyen	circulaire	90 × 90 × 30		galets rubéfiés	27950	
2127	Néolithique moyen	circulaire	100 × 100 × 20		galets rubéfiés	27801	
2129	Néolithique moyen	circulaire	80 × 80 × 31	sédiment encaissant	bloc de molasse rubéfié	27946	
2131	Néolithique moyen	circulaire	70 × 70 × 30		dallettes rubéfiées	27810 et 27831	
2134	Néolithique moyen	circulaire	75 × 75 × 20		galets rubéfiés et blocs thermofractés	27996	
2135	Non daté	circulaire	70 × 70 × 25		galets rubéfiés	27832	
2137	Néolithique moyen	ovale	110 × 85 × 32		galets rubéfiés et bloc	27805	
2139	Non daté	circulaire	60 × 55 × 23		galets rubéfiés		
2140	Non daté	indét.	90 × 50 × 10		galets rubéfiés		
2143	Non daté	ovale	80 × 65 × 14		galets rubéfiés		
2145	Néolithique moyen	circulaire	90 × 90 × 55		galets rubéfiés	27803	
2146	Néolithique moyen	circulaire	100 × 100 × 35		galets rubéfiés	27949	
2149	Non daté	ovale	140 × 100 × 19		galets rubéfiés		
2152	Néolithique moyen	carrée?	110 × 110 × 40		galets rubéfiés et dallettes	27835, 27836 et 27947	
2153	Non daté	ovale	110 × 85 × 17		galets rubéfiés		
2155	Néolithique moyen	circulaire	120 × 120 × 18		galets et blocs rubéfiés	27819 et 27924	
2158	Non daté	circulaire	80 × 80 × 16		galets rubéfiés et blocs thermofractés		
2160	Non daté	circulaire	90 × 85 × 24		galets rubéfiés		
2161	Non daté	circulaire	60 × 60 × 12		galets rubéfiés et blocs thermofractés		
Fosses de combustion							
Structure	Attribution chronologique	Plan	Dimensions [L × l × p en cm]	Rubéfaction	Galets / blocs	Inv. mobilier	Datation ^{14}C calibrée
2017	Epoque romaine	rectangulaire	190 × 96 × 14	sédiment encaissant			153 BC - 63 AD

Fosses de combustion							
Structure	Attribution chronologique	Plan	Dimensions [L × l × p en cm]	Rubéfaction	Galets / blocs	Inv. mobilier	Datation $_{14}$C calibrée
2036	Epoque romaine	circulaire	230 × 208 × 35	comblement et sédiment encaissant		St36	82 - 234 AD
2038	Epoque romaine	rectangulaire	248 × 166 × 29	sédiment encaissant		St38	4 - 131 AD
2039	Néolithique moyen	rectangulaire?	170 ×? × 48	sédiment encaissant		St39	
2044	Mésolithique	ovale?	152 × 82 × 55	sédiment encaissant		St44	7029 - 6647 BC
2085	Epoque romaine	carrée	160 × 160 × 19	sédiment encaissant		27917	75 - 222 AD
2156	Epoque romaine	rectangulaire	160 × 115 × 7	sédiment encaissant		27923	
Foyers en fosse ou rejets							
Structure	Attribution chronologique	Plan	Dimensions [L × l × p en cm]	Rubéfaction	Galets / blocs	Inv. mobilier	Datation $_{14}$C calibrée
1076	Epoque romaine	rectangulaire	100 × 80 × 20			26626	
1104	Non daté: Protohistoire	circulaire	100 × 100 × 35			26652	
2003	Non daté	indét.: deux poches circulaires	120 × 20 × 5				
2004	Non daté	ovale	65 × 58 × 8				
2007	Non daté	ovale	82 × 64 × 20		galets rubéfiés		
2010	Non daté	ovale	106 × 74 × 19			St10	
2013	Non daté	ovale	70 × 60 × 4				
2016	Non daté	ovale	112 × 86 × 13	sédiment encaissant		St16	
2021	Non daté	circulaire	72 × 70 × 25				
2024	Non daté	rectangulaire	80 × 68 × 14			St24	
2025a	Non daté	indét.	114 × 64 × 8				
2032	Epoque romaine	carrée	74 × 70 × 15			St32	
2033	Epoque romaine	ovale	160 × 136 × 23				162 BC - 46 AD
2042	Epoque romaine	rectangulaire	142 × 110 × 22	sédiment encaissant			245 - 389 AD
2043	Néolithique moyen	rectangulaire	90 × 70 × 26			St43	3956 - 3715 BC
2050	Non daté	rectangulaire	54 × 44 × 10	sédiment encaissant			
2053	Non daté	rectangulaire	52 × 40 × 10	sédiment encaissant		St53	
2057	Non daté	ovale	60 × 50 × 16				
2058	Non daté	carrée	68 × 66 × 18				
2060	Néolithique moyen	ovale	94 × 64 ×?			St60	
2061	Non daté	ovale	70 × 60 × 10				
2065	Non daté	ovale	96 × 70 × 27	sédiment encaissant			

Foyers en fosse ou rejets							
Structure	Attribution chronologique	Plan	Dimensions [L × l × p en cm]	Rubéfaction	Galets / blocs	Inv. mobilier	Datation $_{14}$C calibrée
2070	Non daté	ovale	74 × 48 × 8				
2071	Non daté	circulaire	80 × 74 × 11				
2072	Non daté	ovale	64 × 40 × 12				
2075	Bronze final	rectangulaire	90 × 47 × 5				1000 - 830 BC
2076	Non daté	indét.	? × 35 × 17				
2079	Non daté	ovale	90 × 80 × 15			27821	
2084	Non daté	circulaire	70 × 70 × 8				
2088	Non daté	circulaire	60 × 60 × 10				
2094	Non daté	circulaire	40 × 40 × 8				
2095	Non daté	polylobée	45 × 45 × 6				
2096	Non daté	carrée	82 × 80 × 15				
2098	Non daté	indét.	80 × 45 × 1			27824	
2113	Epoque romaine	rectangulaire	128 × 72 × 13				141 - 334 AD
2114	Non daté	ovale	70 × 50 × 18				
2116	Non daté	circulaire	40 × 40 × 12				
2119	Non daté	circulaire	45 × 45 × 8				
2136	Non daté	ovale	70 × 60 × 10				
2138	Epoque romaine	rectangulaire	160 × 100 × 15				78 - 224 AD
2141	Non daté	ovale	55 × 35 × 12				
2142	Néolithique moyen	carrée?	70 × 70 × 17			27834	
2144	Non daté	ovale	100 × 67 × 10				
2151	Non daté	ovale	22 × 10 × 5				
2157	Non daté	polylobée	35 × 30 × 14				
2159	Non daté	circulaire	40 × 40 × 15				

ANNEXE 8 Catalogue synthétique des structures à fonction indéterminée.

Structure	Attribution chronologique	Type	Plan	Dimensions [L × l × p en cm]	Inv. mobilier
1107	Epoque romaine	Trou de poteau?	circulaire, profil en V	40 × 40 × 24	26647
2091	Néolithique moyen	Fosse à remplissage ocre	bilobée ou deux poches contiguës	221 × 125 × 18	27912

ANNEXE 9 Analyse de mobilier métallique au MEB

André Piuz[1]

L'objectif de cette étude est de déterminer que les objets soumis à l'analyse sont bien composés d'un alliage de Cu et de Sn, soit du bronze à l'étain. La méthode utilisée est qualitative et ne permet pas d'obtenir des données quantitatives précises sur la proportion des éléments de base et des impuretés présentes.

Les analyses et images ont été effectuées au Muséum d'histoire naturelle de la ville de Genève sur un MEB (microscope électronique à balayage) Zeiss® DSM940a équipé d'un analyseur EDX (*energy dispersive spectrometry*) Noran® System Six sur les objets non métallisés.

Les échantillons étudiés proviennent des tombes St. 1052 et 1061. Pour la première, il s'agit d'une épingle [26635-1], d'un annelet [26635-2] et d'un rasoir [26635-3]. Pour la seconde, ce sont un annelet et un anneau de cheville [26636-6] qui ont été soumis à l'analyse.

Afin de de déterminer la composition des cinq objets étudiés, les analyses, qualitatives, ont été effectuées sur différentes régions à la surface de chaque échantillon. Généralement, ces analyses ont été réalisées sur la patine verdâtre (croute d'altération d'aspect souvent grumeleux) ainsi que parfois sur des surfaces plus lisses ou à travers des « fenêtres » permettant d'observer le matériau situé au-dessous de la (première) couche d'altération. Il est à noter qu'une section polie à travers l'objet étudié serait indispensable à l'obtention d'une bonne analyse de l'alliage originel afin d'éviter les biais liés au profil d'oxydation induisant des changements de composition en fonction de la profondeur. Nous pouvons donc considérer ici que la totalité des analyses ont été effectuées sur des surfaces plus ou moins altérées qui ne représentent pas la composition de l'alliage original.

EPINGLE [ST. 1052, 26635-1]

Les analyses (1a, 1c) effectuées sur la patine d'altération montrent des teneurs en étain plus grandes qu'en cuivre (Sn>Cu), indiquant un lessivage du cuivre. Une analyse (1b) indique une teneur en cuivre beaucoup plus importante que l'étain (Sn<Cu) qui peut soit résulter de la dissolution de l'étain, soit s'approcher de la composition du bronze constituant l'épingle.

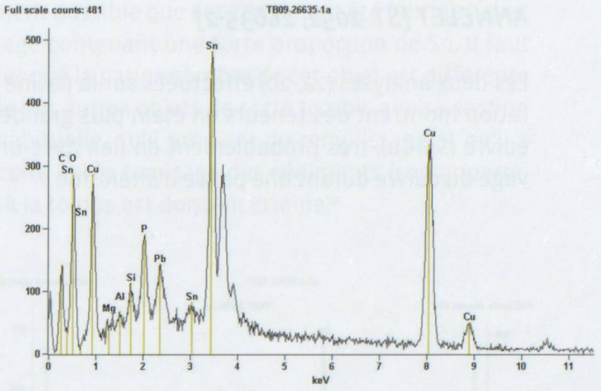

1a

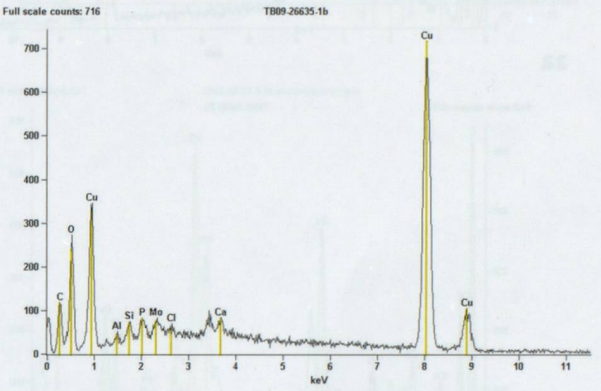

1b

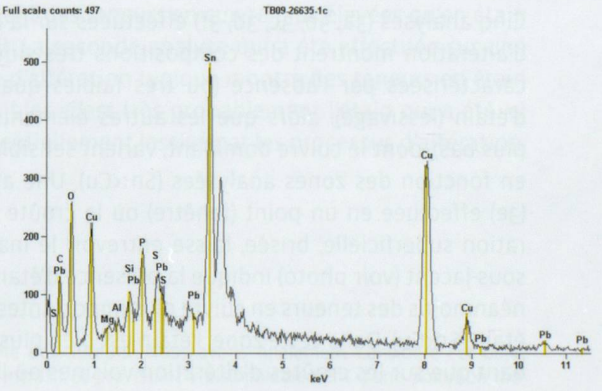

1c

1 Département de microscopie électronique, Muséum d'histoire naturelle, Genève.

ANNELET [ST. 1052, 26635-2]

Les deux analyses (2a, 2b) effectuées sur la patine d'altération montrent des teneurs en étain plus grande qu'en cuivre (Sn>Cu), très probablement en lien avec un lessivage du cuivre durant une phase d'altération.

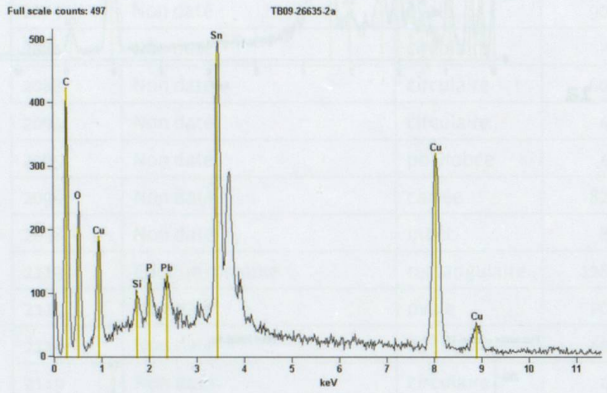

2a

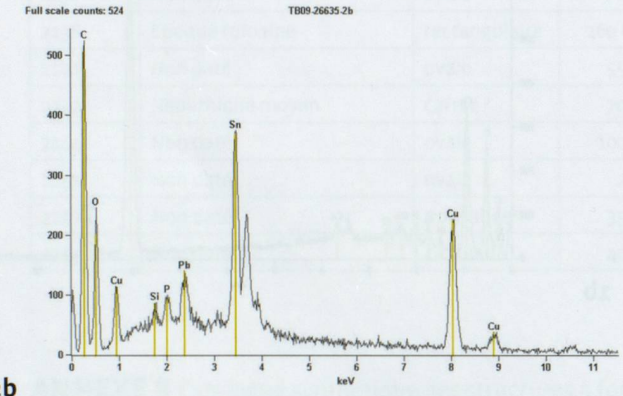

2b

RASOIR [ST. 1052, 26635-3]

Cinq analyses (3a, 3b, 3c, 3d, 3f) effectuées sur la croûte d'altération montrent des compositions très similaires caractérisées par l'absence (ou très faibles quantités) d'étain (lessivage), alors que les autres éléments (voir plus bas), dont le cuivre dominant, varient sensiblement en fonction des zones analysées (Sn<<Cu). Une analyse (3e) effectuée en un point (fenêtre) où la croûte d'altération superficielle, brisée, laisse entrevoir le matériau sous-jacent (voir photo) indique la présence d'étain avec néanmoins des teneurs en cuivre plus importantes qu'en étain (Sn<Cu). Dans cette zone, l'étain est bien plus abondant que sur les croûtes d'altération voisines où il n'a le plus souvent pas été détecté.

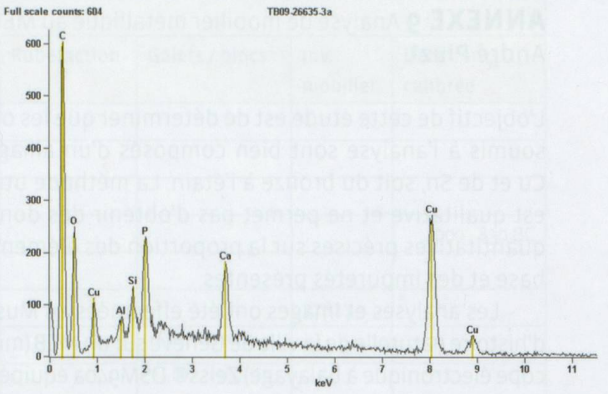

3a

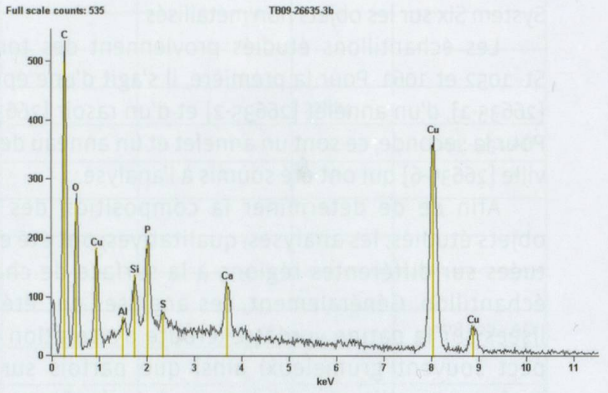

3b

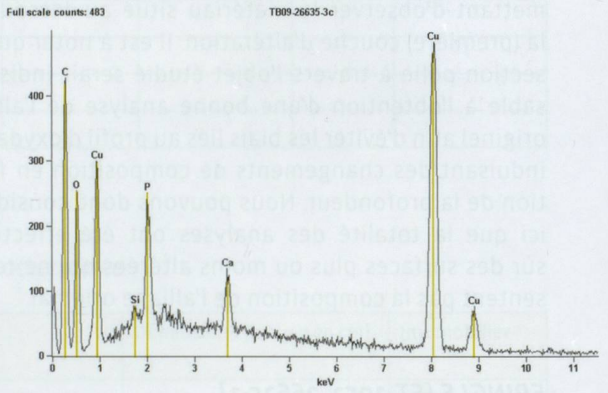

3c

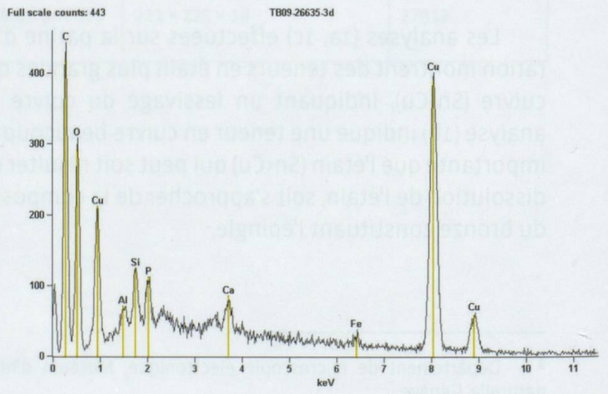

3d

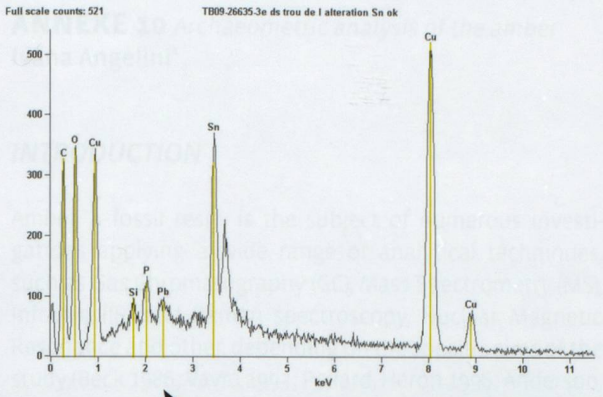

3e

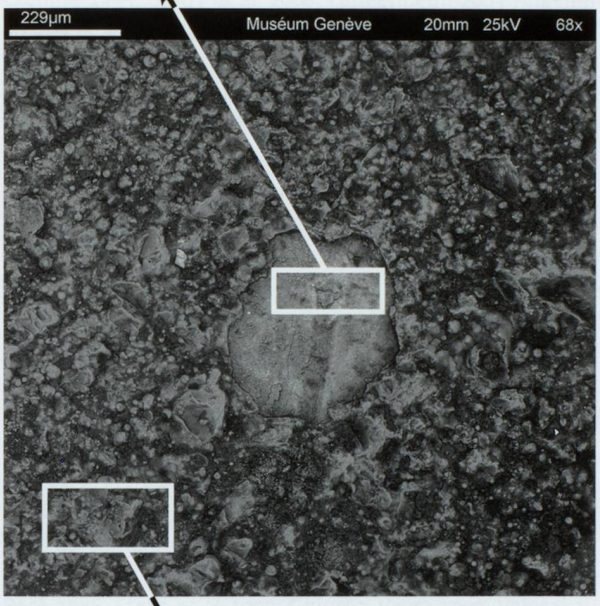

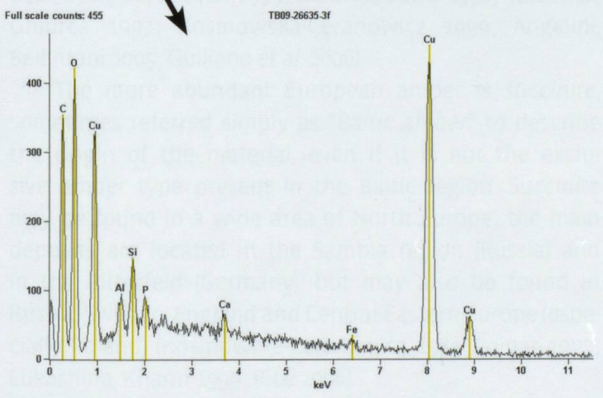

3f

ANNELET [ST. 1061]

Les deux analyses (4a, 4b) effectuées sur cet objet indiquent des teneurs en étain plus grandes qu'en cuivre (Sn>Cu). Ce dernier élément pourrait avoir été en grande partie lessivé par les processus d'altération. Mais il est également possible que cet annelet ait été fabriqué avec un alliage contenant une forte proportion de Sn. Il faut rappeler que la patine sombre de cet objet est différente de celle des autres objets de cette tombe, que sa section est inhabituelle, qu'il provient du remplissage et qu'il a été récolté après tamisage des sédiments (son appartenance à la tombe est donc incertaine)[2].

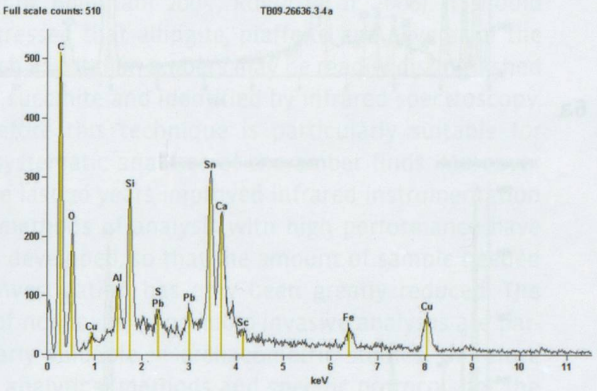

4a

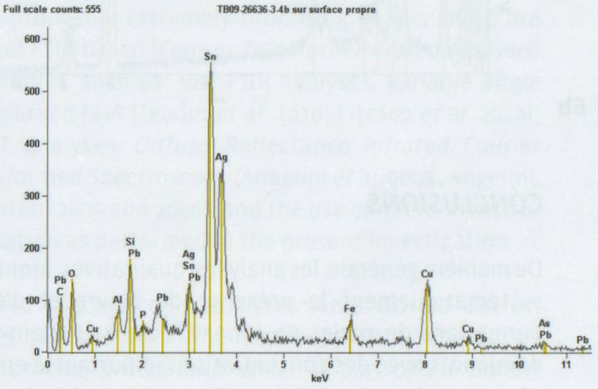

4b

ANNEAU DE CHEVILLE [ST. 1061, 26636-6]

Les deux analyses (6a, 6b) effectuées sur cet objet indiquent des teneurs en cuivre plus élevées qu'en étain (Sn<Cu). La seconde analyse qui a été effectuée sur une croûte d'altération typique montre des teneurs en étain très faibles. C'est très probablement l'étain qui a été ici préférentiellement lessivé par les processus d'altération.

2 Note des auteurs: Nous avons finalement considéré cet objet comme intrusif et provenant vraisemblablement d'une pollution moderne. Il n'a pas été conservé.

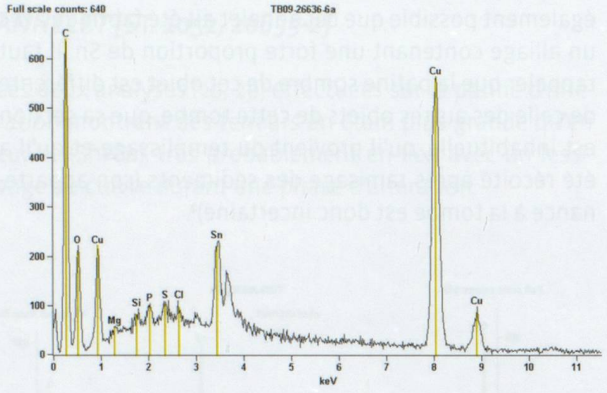

6a

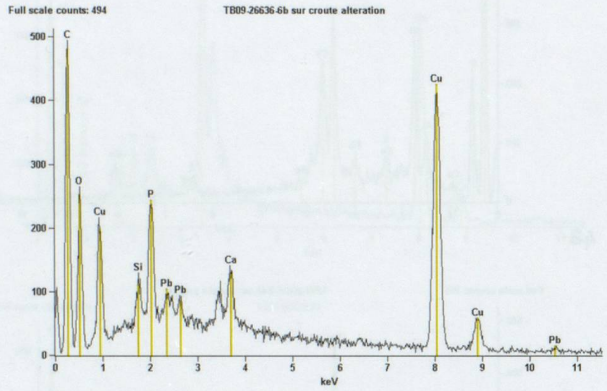

6b

CONCLUSIONS

De manière générale, les analyses, qualitatives, montrent systématiquement la présence de cuivre et d'étain permettant de parler de bronze. Cuivre et étain sont dominants avec des concentrations importantes en oxygène et carbone (possibles carbonates), accessoirement accompagnée de plomb, argent, aluminium, phosphore, magnésium, aluminium, silicium, calcium, fer et soufre (possibles sulfates). Si certains de ces éléments, analysés à la surface des objets, sont certainement des éléments accessoires du bronze, d'autres peuvent être des restes de la matrice (sol, nappe phréatique) qui contenait les objets avant leur découverte. Il semble exister ici deux types de produits d'altérations (voir Robbiola et Hurtel 1991, Piccardo et Mille 2007 *cum biblio*): ceux contenant de grandes quantités de composés de l'étain (Sn>Cu, Epingle, deux Annelets), et ceux essentiellement constitués par des composés du cuivre (Sn<Cu, Rasoir, Anneau de cheville). Les raisons de ces deux produits d'altération restent à discuter mais la composition originale des alliages des différents échantillons (qui nécessiterait la confection de sections polies à travers les objets) serait alors nécessaire.

ANNEXE 10 *Archaeometric analysis of the amber*

Ivana Angelini[1]

INTRODUCTION

Amber, a fossil resin, is the subject of numerous investigations applying a wide range of analytical techniques, such as Gas Chromatography (GC), Mass Spectrometry (MS), Infrared (IR) and Raman spectroscopy, Nuclear Magnetic Resonance and other, depending on the specific aims of the study (Beck 1986; Vavra 1993; Pollard, Heron 1996; Anderson, Crelling 1995; Brody *et al.* 2000; Langenheim 2003 Angelini 2010a). IR spectroscopy is specifically used in the identification of the nature and origin of the amber material, thanks to the low cost and low invasive approach of the technique, which also shows a high sensitivity in the determination of the amber source. Indeed, since the '60 Beck and co-workers proved that succinite, the more abundant type of amber of Baltic origin, exhibits characteristic infrared spectra differing from all other amber signatures (Beck *et al.* 1964 and 1965; Beck 1970). Actually, a few North American ambers have rather similar IR spectra (Langenheim 1969; Rice 2006), but this is not a problem for the study of the archaeological ambers, and it is an issue only in the investigation of modern materials. Even if not all the amber types exhibit a unique spectrum that could identify unambiguously the source, the large number of studies carried out to date allow to identify the IR signature of a large variety of amber-types, such as: rumanite, simetite, gedanite, gedano-succinite and many others (reference literature: Beck, Hartnett 1993; Beck 1986; Stout *et al.* 1995; Ghiurca, Vavra 1990; Valaczkai, Ghiurca 1997; Kosmowska-Ceranowicz 1999; Angelini, Bellintani 2005; Guiliano *et al.* 2006).

The more abundant European amber is *succinite*, sometimes referred simply as "*Baltic amber*" to describe the origin of the material, even if it is not the exclusive amber type present in the Baltic region. *Succinite* may be found in a wide area of North Europe; the main deposits are located in the Sambia region (Russia) and in the Bitterfeld (Germany), but may also be found in Russia, Sweden, England and Central-Eastern Europe (especially Poland) (Kosmowska-Ceranowicz 1984 Poinar 1992; Lukashina, Kharin 1999; Rice 2006).

Europe is also characterized by the presence of a large number of amber types having different age and composition, and may be found in small deposits widespread in many countries, such as Spain, French, Germany, Austria, Swiss, Italy, Hungary and Romania. Allingite and plaffeite are the two amber-types typical of Switzerland (Beck 1986; Beck, Stout 2000; Beck *et al.* 1993), although in order to study the origin of archaeological Swiss amber it is important to consider the amber deposits located in Southern France (ad example: Beck, Liu 1976; Guiliano *et al.* 2006) and in Northern-Central Italy (Veggiani 1952; Dalrio 1980; Skalsky, Veggiani 1990; Boscardin, Tescari 1996; Trevisani *et al.* 2005; Giannola *et al.* 1998; Angelini, Bellintani 2005; Roghi *et al.* 2006). It should be stressed that allingite, plaffeite and several of the French and Italian ambers may be readily distinguished from succinite and identified by infrared spectroscopy. Therefore this technique is particularly suitable for the systematic analyses of the amber finds. Moreover in the last 20 years improved infrared instrumentation and methods of analysis with high performance have been developed, so that the amount of sample needed for investigation has now been greatly reduced. The use of non-invasive or micro-invasive analyses are particularly valuable in archaeometric studies, therefore such analytical methods and specific protocols for the investigation of amber archaeological artefacts have been proposed. Extremely promising in this sense are several FTIR-based (*Fourier Transform Infrared Analysis*) techniques, such as: VAR-FTIR analyses, *Variable Angle Reflectance-FTIR* (Teodor *et al.* 2010; Litescu *et al.* 2012); DRIFT analyses, *Diffuse Reflectance Infrared Fourier Transformed Spectroscopy* (Angelini *et al.* 2003; Angelini, Bellintani 2005 and 2006); and the use of micro-IR instrumentation as performed in the present investigation.

Infrared spectroscopic analyses were carried out on amber beads found in the necropolis of Tolochenaz VD - *La Caroline*, Switzerland, which is part of the *Boiron* necropolis, and dated to the Final Bronze Age (FBA). The results are here presented and discussed in comparison with the data from the archaeometric literature.

MATERIALS AND METHODS

Thirty two beads from graves: St. 1018 (2 beads), St. 1061 (6 beads), St. 1084 (23 beads) and St. 1086 (1 bead) were selected for the analytical investigations. The initial phase of the work included the classification of the finds and the determination of the main physical properties: dimensions (measured by a caliper), weight and color. The colors were described also by the use of the *Natural Color System* (NCS) tables, which may be easily converted in the *Munsell Color System* codes. All the data, the labels of each bead used during the analyses and the relative inventory number are listed in **fig. 1**.

1 Département de Géoscience, Université de Padova, Italie.

Label	Typology	Dimensions [mm]	Color/materials	NCS color code	Weight [g]	Classification data	Sampling area
Boi-C1a	Cylindrical bead	Dest= 7.0; Dint= 3.5; H= 3.2	Surface with dark orange patina	S2060-Y20R	0.089	T. 1061, N° inv. 26636-3.1	In an area where is lost the thick patina of weathering
Boi-C1b	Cylindrical bead	Dest= 7.2; Dint= 3.1; H= 3.4	Surface with dark orange patina	S2060-Y30R	0.081	T. 1061, N° inv. 26636-3.1	In an area where is lost the thick patina of weathering
Boi-Fr1a	Fragment of cylindrical bead	Lmax= 8.6; Lint= 5.2; H=3.8	Weathering patina: dark orange-brown. Amber: dark orange-red	Patina:S2060-Y20R; Inner amber: S2060-Y60R	0.073	T. 1061, N° inv. 26636-3.1	From a lateral fracture
Boi-Fr1b	Fragment of cylindrical bead	Lmax= 6.3; Lint= 3.2; H=4.2	Weathering patina: dark orange-brown. Amber: dark orange-red	Patina: S2050-Y20R; Inner amber: S2060-Y60R	0.050	T. 1061, N° inv. 26636-3.1	From a lateral fracture
Boi-Fr1c	Fragment of cylindrical bead	Lmax= 6.5; Lint= 3.0; H= 4.0	Weathering patina: dark orange-brown. Amber: dark orange-red	Patina: S2060-Y20R; Inner amber: S2050-Y40R	0.038	T. 1061, N° inv. 26636-3.1	From a lateral fracture
Boi-Fr1d	Fragment of cylindrical bead	Lmax= 3.3; H=3.3	Weathering patina: dark orange. Amber: dark red	Patina: S2050-Y20R; Inner amber: S2060-Y50R	0.012	T. 1061, N° inv. 26636-3.1	From a lateral fracture
Boi-C8a	Fragment of cylindrical bead	Large frag.: Lmax=5.3; H=2.0 Medium frag.: Lmax=3.5; H=1.8 Small frag. Lmax= 3.2; H=1.7	Amber: dark orange-red. Surface area with pale orange weathering patina	S3040-Y40R	0.032	T. 1018, N° inv. 26634-6	From a lateral fracture
Boi-C8b	Cylindrical bead	Dest= 8.35; Dint= 2.5; H= 4.0	Dark orange-brown surface. Some weatherd area are pale orange	S3050-Y40R	0.149	T. 1018, N° inv. 26634-2	From a surface fracture
Boi-C4-1	Cylindrical bead	Dest= 9.3; Dint= 3.5; H= 2.6	Weathering patina: dark orange-brown. Amber: dark red	S3060-Y30R	0.134	T. 1084, N° inv. 26642-1	From a surface fracture on a side of the bead
Boi-C4-2a	Cylindrical bead	Dest= 12.0; Dint= 4.0; H= 6.1	Brown surface	S4050-Y40R	0.566	T. 1084, N° inv. 26642-2a	Sampling with a needle from the inner of the perforation
Boi-C4-2b	Cylindrical bead	Dest= 8.2; Dint= 3.5; H= 4.5	Dark orange-pale brown surface	S3050-Y30R	0.145	T. 1084, N° inv. 26642-2b	Sampling with a needle from the inner of the perforation
Boi-C4-2c	Cylindrical bead	Dest= 11.4; Dint= 4.2; H= 1.2	Pale brown surface	S4050-Y30R	0.453	T. 1084, N° inv. 26642-2c	Sampling with a needle from the inner of the perforation
Boi-C4-3	Cylindrical bead	Dest= 8.4 Dint= 4.2; H= 4.0	Dark orange-pale brown surface	S2570-Y30R	0.140	T. 1084, N° inv. 26642-3	From a small surface fracture
Boi-C4-4	Incomplete cylindrical bead	Dest= 10.2; Dint= 2.8; H= 4.4	Dark orange-pale brown surface	S3050-Y40R	0.246	T. 1084, N° inv. 26642-4	Sampling with a needle from the inner of the perforation
Boi-C4-5	Cylindrical bead	Dest= 12.0; Dint= 3.9; H= 7.7	Some areas are dark brown, others are dark orange	S2060-Y40R	0.627	T. 1084, N° inv. 26642-5	From a lack of material, near the perforation
Boi-C4-6	Cylindrical bead	Dest= 13.5; Dint= 3.8; H= 11.9	Orange surface with red-brown areas	S2060-Y40R	0.757	T. 1084, N° inv. 26642-6	From a lack of material on a side of the bead
Boi-C4-7	Cylindrical bead	Dest= 13.0; Dint= 4.1; H= 8.5	Dark orange-brown surface	S2070-Y30R	0.792	T. 1084, N° inv. 26642-7	Sampling with a needle from the inner of the perforation
Boi-C4-8	Cylindrical bead	Dest= 11.7; Dint= 4.3; H= 6.6	Orange surface with dark red areas	S2070-Y30R	0.494	T. 1084, N° inv. 26642-8	From a lack of material, near the perforation
Boi-C4-9	Cylindrical bead	Dest= 10.3; Dint= 3.8; H= 7.2	Orange surface with dark red areas	S4050-Y30R	0.385	T. 1084, N° inv. 26642-9	Close to the perforation
Boi-C4-10	Cylindrical bead	Dest= 10.5; Dint= 3.1; H= 5.8	Dark orange-brown surface. Wheathered spotted areas: black spots and white zone (due to the conservant)	Patina: S3050-Y30R Inner amber: S2570-Y40R	0.304	T. 1084, N° inv. 26642-10	From a fracture on a side of the bead
Boi-C4-11	Cylindrical bead	Dest= 11.1; Dint= 3.8; H= 5.8	Dark orange-brown surface	S3050-Y30R	0.431	T. 1084, N° inv. 26642-11	Sampling with a needle from the inner of the perforation
Boi-C4-12	Cylindrical bead	Dest= 7.7; Dint= 3.7; H= 3.2	Dark brown-red surface	S3050-Y30R	0.105	T. 1084, N° inv. 26642-12	Sampling with a needle from the inner of the perforation
Boi-C4-13a	Cylindrical bead	Dest= 8.0; Dint= 3.0; H= 4.5	Orange surface with black areas due to soil glued by the conservant	S2060-Y30R	0.168	T. 1084, N° inv. 26642-13a	Sampling with a needle from the inner of the perforation
Boi-C4-13b	Cylindrical bead	Dest= 8.2; Dint= 3.4; H= 4.7	Orange surface with black areas due to soil glued by the conservant	S2060-Y40R	0.157	T. 1084, N° inv. 26642-13b	Sampling with a needle from the inner of the perforation
Boi-C4-13c	Cylindrical bead	Dest= 10.0; Dint= 3.4; H= 4.6	Brown surface	S2070-Y20R	0.288	T. 1084, N° inv. 26642-13c	From a lack of material in the inner of the perforation
Boi-C4-13d	Cylindrical bead	Dest= 7.7; Dint= 2.5; H= 4.2	Dark orange-brown surface	S3060-Y40R	0.150	T. 1084, N° inv. 26642-13d	Sampling with a needle from the inner of the perforation
Boi-C4-13e	Cylindrical bead	Dest= 8.2; Dint= 2.8; H= 4.0	Dark orange-brown surface	S2070-Y20R	0.147	T. 1084, N° inv. 26642-13e	Sampling with a needle from the inner of the perforation
Boi-C4-13f	Cylindrical bead	Lmax= 6.4; Lint= 3.1; H= 3.0	Dark orange surface	S2070-Y20R	0.045	T. 1084, N° inv. 26642-13f	From a lateral fracture
Boi-C4-13g	Cylindrical bead	Dest= 7.0; Dint= 3.1; H= 2.7	Dark orange surface	S2070-Y40R	0.078	T. 1084, N° inv. 26642-13g	Sampling with a needle from the inner of the perforation
Boi-C4-13h	Cylindrical bead	Dest= 7.5; Dint= 3.6; H= 3.0	Dark orange-brown surface	S3060-Y40R	0.082	T. 1084, N° inv. 26642-13h	From a surface fracture
Boi-C4-13i	Cylindrical bead	Dest= 7.3; Dint= 4.6; H= 3.3	Dark orange-brown surface	S2070-Y30R	0.061	T. 1084, N° inv. 26642-13i	From a surface fracture
Boi-L6	Spherical bead with flattened poles and irregular thickness	Dest= 20.0; Dint= 5.0; H= 9.4	Weathered dark orange-reddish surface	S4030-Y50R	2.012	T. 1086, N° inv. 26650-2	A small splinter lost from the surface and present in the conservation bo

Fig. 1. Summary of the analysed amber beads with relative sampling areas, bead typology, physical characteristics (weight, dimension, colour and NCS colour code –Natural Colour System), the grave code (T) and classification number (N° inv.). [Dest = external diameter the bead; Dint= diameter of the hole; H = height].

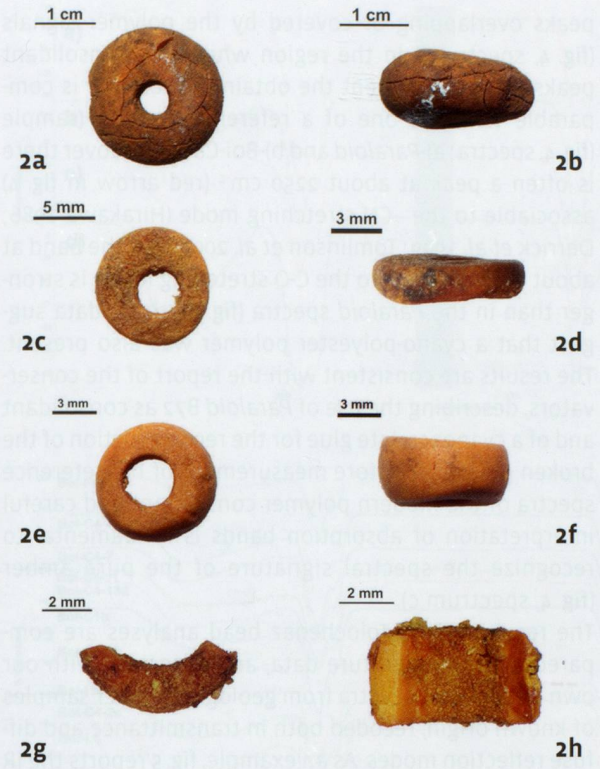

Fig. 2. Examples of the bead typologies analysed, as described in fig. 1. Zenithal and lateral images of the beads with dimensional scales: a-b) Boi-L6; c-d) Boi-C4-1; e-f) Boi-C4-2a; g-h) Boi-Fr1c.

Fig. 3. Details of selected surfaces of the analysed beads, recorded by a stereomicroscope (magnification 8-20 X): a) bead Boi-C8a: thick pale orange weathered crust and inner unweathered red amber; b) bead Boi-C1b: weathered surface with extensive crackle and a thick layer of polymer consolidant producing the "glassy" aspect; c) bead Boi-C4-2a: deep cracks filled with consolidant and grains of weathered amber; d) bead Boi-L6: loss of material from an intensively fissured area.

The bead typologies, also reported in **fig. 1**, are extremely simple: all but one are cylindrical beads, showing variable height and thickness (**fig. 2,c-h**). The finds are small with an external diameter generally around 10 mm, only a few beads have a diameter in the range of 10-13 mm. The only large bead is sample Boi-L6 that is a spherical bead with flattened poles and irregular thickness, with a diameter of 20 mm (**fig. 2,a-b**). For a detailed study of the statistical distribution of weight and dimension of the beads, and the comparison with similar bead typologies see chap. 4.7.3 in this volume.

The amber finds were studied in details by Optical Microscopy (OM), using a stereo-microscope Nikon SMZ 645, equipped with a led circular Photonic Optics illumination and a Nikon Coolpix 6.1 digital camera, for the microphotography recording. The principal aim of the OM analysis is the investigation of the surface conservation state of the ambers in order to choose the proper area for the sampling. In previous archaeometric study of amber DRIFT analyses were systematically used yielding excellent results (for example: Angelini, Bellintani 2005 and 2006, Angelini 2009a, 2010b, 2012 and 2013). Therefore it was planned to use the same technique for the investigation of the ambers from *La Caroline*. In order to perform a DRIFT analyses 0.2 mg of amber sample are sufficient, although the technique is highly sensitive to impurities therefore the sample has to be "pure", i.e. without soil contamination or any trace of polymer consolidant. Moreover, especially with small objects, it is important to minimize the removed amount of material in order to avoid aesthetical damages. For these reasons the sampling operation is extremely critical and the preliminary examination of the amber surface and morphology is important.

The majority of the finds from *La Caroline* show a thick patina composed by weathered amber having a completely different colour and consistence with respect to the inner original amber, as clearly visible in several broken beads (**fig. 3,a**). The weathered amber surfaces may exhibit severe crackle (**fig. 3,b**) and/or deep cracks (**fig. 3,c**), which in some cases may lead to the loss of material (**fig. 3,d**). Samples for the spectroscopic analyses were cut by the use of a steel blade or needle from pre-existing fractures (such as in **fig. 3,a.d**), or from within the perforation (**fig. 2**). The amount of amber sampled from each bead is about 0.2-0.3 mg.

Due to the poor surface preservation it was impossible to observe use-wears marks related to the production and/or to the use of the beads.

The beads from *La Caroline* underwent restoration before the analytical study. The OM investigation showed clearly that the applied polymer consolidant penetrated deep into the beads, sometimes –accumulating as a thick surface

layer producing a glassy effect (**fig. 3,b**). In several beads soil remains and mineral grains are embedded or attacked to the amber surface through the adhesive effect of the consolidant (**fig. 2,g-h**).

Taking into account the conservation state of the amber beads and the presence of substantial quantity of consolidant on the surface and in the fractures, it was virtually impossible to obtain pure amber samples, therefore it was necessary to select a different type of IR analysis: instead of normal DRIFT analysis, it was decided to work in Micro-FTIR conditions. The instrument used is located in the Laboratories of the Institute for Energy and Interphases, Italian National Research Council (IENI-CNR), and was made available for the analyses thanks to the collaboration with Dr Monica Favaro. The measurements were performed by a Continuum Nicolet microscope connected to a Thermo-Fischer IS-10 system and equipped with a Mercury Cadmium Telluride (MCT) detector. The spectra were recorded in reflectance mode in the 650–4000 cm^{-1} spectral range, working with a resolution of 4 cm^{-1} and accumulation of 64 scans. The advantage of this method is that a very small fragment of amber (<0.1 mg) is needed for the analysis. The amber sample is powdered and deposited on a microscope slide (MirrIR Kevley Technology) by manual pressing and rolling on the surface. Each IR analysis is obtained from an area of about 10-15 × 10-15 μm^2, and several spectra are recorded from the same sample in order to isolate the clear signal of the amber.

RESULTS AND DISCUSSION

The analyses of the Tolochenaz VD - *La Caroline* amber beads was particularly difficult due to the heavy contamination of the amber material with the consolidant and glue used for the restauration. The recorded spectra in the majority of the cases show the amber absorption peaks overlapping or covered by the polymer signals (**fig. 4**, spectrum). In the region where the consolidant peaks are more evident the obtained spectrum is comparable with the one of a reference *Paraloid* sample (**fig. 4**, spectra: a)-*Paraloid* and b)-Boi-C8b). Moreover there is often a peak at about 2250 cm^{-1} (red arrow in **fig. 4**) associable to the –CN stretching mode (Hirakawa 1986; Derrick *et al.* 1999; Tomlinson *et al.* 2006) and the band at about 1250 cm^{-1} due to the C-O stretching mode is stronger than in the *Paraloid* spectra (**fig. 4**): these data suggest that a cyano-polyester polymer was also present. The results are consistent with the report of the conservators, describing the use of *Paraloid* B72 as consolidant and of a cyanoacrylate glue for the reconstruction of the broken pieces. Therefore measurement of the reference spectra of the modern polymer consolidant and careful interpretation of absorption bands is fundamental to recognize the spectral signature of the pure amber (**fig. 4**, spectrum c).

The results of the Tolochenaz bead analyses are compared with the literature data, and especially with our own database of spectra from geological amber samples of known origin, recoded both in transmittance and diffuse reflection modes. As an example, **fig. 5** reports the IR spectra of four reference amber samples: a plaffeite, two succinites and one rumanite from the Coltzi; the different amber types may be easily discriminated.

The 32 analysed beads display similar absorption peaks: the ten samples reported in **fig. 6** are representative. Strong absorptions related to the stretching and bending vibrations of the $-CH_2$ and $-CH_3$ g.oups are visible at about 2930, 2870, 1455 and 1375 cm^{-1}, whereas the intense peak associated to the carbonyl stretching is recorded in the range 1715- 1730 cm^{-1}. The spectral region at 1200-800 cm^{-1} is often called the "fingerprint region", it exhibits a strong peak at about 1160 cm^{-1} preceded by a broad band (called "Baltic shoulder"), due to the C-O bond stretching

Fig. 4. Comparison of IR spectra of: a) reference *Paraloid* sample; b) spectrum of the surface of bead Boi-C8b showing the absorption peaks of amber overlapping with those of *Paraloid* and of a cyanoacrylate polymer, and c) spectrum of amber of bead Boi-C8b showing the typical signal of succinite.

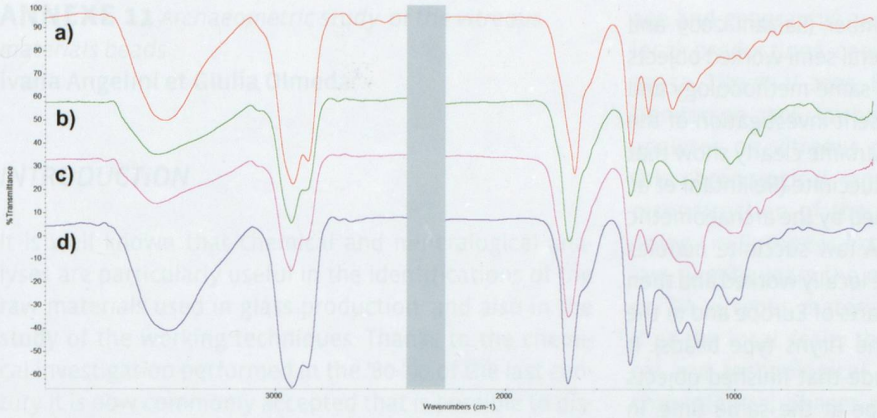

Fig. 5. IR spectra from some reference amber from geological samples: a) plaffeite; b) and c) succinite from different places; d) rumanite (The grey area is the one characteristic of the CO_2 peaks).

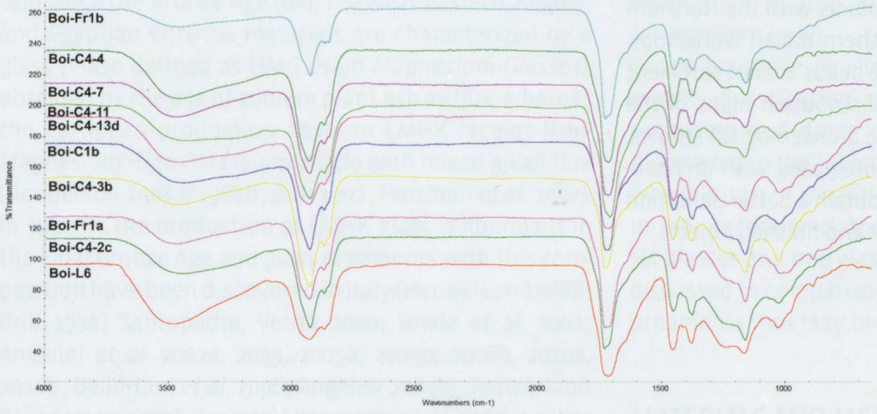

Fig. 6. IR spectra of selected samples, obtained by reflective infrared analyses with a micro-infrared instrument. All the samples show the typical spectrum of succinite.

of the saturated esters. Other two important peaks are recorded at about 990-1000 cm^{-1} and 885-890 cm^{-1} related respectively to the symmetric bending of cyclohexane C-H bonds and to the bending out of plane of the terminal C-H olefinic bonds (Beck *et al.* 1965; Larsson 1978; Cozzi *et al.* 1997; Derrick *et al.* 1999). The latter absorption peak is generally weak and sometimes absent due to the oxidation of the terminal olefinic double bonds. This is characteristic of the weathered amber and is typically found in archaeological ambers (Beck *et al.* 1965; Larsson 1978). All the described features of the spectra allow to identify unambiguously the samples as *succinite*.

CONCLUSIONS

The analytical investigation of the archaeological amber objects in the literature indicate that succinite is the prevalent type of amber used in the past, although recent analyses indicate that, even if rare, a minor use of local amber sources is present through time: from the Palaeolithic, as the case of the La Garma materials (Peñalver *et al.* 2007) to the Roman age, when also the small outcrops of siegburgite were locally used (Dietz *et al.* 2014).

The Swiss amber deposits of allingite and plaffeite seem not to be exploited in ancient times. The results by infrared investigation of about six hundred Leponti amber finds dated to the VI-II centuries BC (Beck, Stout 2000), and the archaeometric study of the Final Bronze Age finds from Hauterive-Champréveyres (Beck *et al.* 1993), together with the present data on the Tolochenaz necropolis clearly indicate that the Swiss archaeological amber finds result invariably composed of succinite.

Numerous infrared analyses are available for North Italian ornaments dated to FBA and the data show that only succinite was present in this area (Angelini, Bellintani 2005 and 2006; Angelini 2009a, 2010b and 2013), whereas during the FBA the use of different amber types is proven in other geographic areas, such as for the Romanian hoard from Cioclovina (Teodor *et al.* 2010), and for some Sicilian objects (our unpublished data). Interestingly, in the Eastern Po Valley a settlement dated to the end of the XIII – beginning of the XII century BC was recently discovered, where a huge amount of unfinished beads, semi-worked objects, amber nucleus and thousands of amber splinters securely

indicate the local working of amber (Salzani 2009 and 2011). The infrared analyses of several semi-worked objects and splinters performed with the same methodology and instrumentation used for the present investigation of the ambers from Tolochenaz VD - *La Caroline* clearly show that the worked amber material was succinite (Bellintani *et al.* in press). The general picture defined by the archaeometric data indicate that during the FBA raw succinite nodules arrived in Northern Italy, they were locally worked and then traded / exchanged in the other parts of Europe and in the Mediterranean region (such as the Tiryns type beads). It is of course not possible to exclude that finished objects also arrived from Northern Europe at the same time. In Switzerland during the FBA only succinite is present, possibly arriving both from direct contacts with the Northern areas of Europe or from the Northern Italian workshops. The rather simple typologies of the beads are not sufficient to obtain useful information by distribution maps of the ornaments. Future progress in the archaeological studies, if systematically combined and integrated with archaeometric investigation, may help to obtain a better definition of the trading routes of raw amber and finished objects.

ANNEXE 11 *Archaeometric study of the vitreous materials beads*

Ivana Angelini et Giulia Olmeda[1]

INTRODUCTION

It is well known that chemical and mineralogical analyses are particularly useful in the identifications of the raw materials used in glass production, and also in the study of the working techniques. Thanks to the chemical investigation performed in the '80-'90 of the last century it is now commonly accepted that is possible to distinguish a European local tradition in the glass production since the Bronze Age (BA). The Near Eastern, Aegean and Egyptian vitreous materials are characterized by a glass phase defined as HMG (*High Magnesium Glasses*), obtained by the use of sodium plant ash as flux, whereas the European production have an LMHK receipt (*Low Magnesium High Potassium*) made with mixed alkali flux (Henderson 1988a, 1988b; Brill 1992; Hartman *et al.* 1997). In specific the production of LMHK glass is abundant in the Final Bronze Age and glass ornaments with this composition have been discovered in Italy (Henderson 1988b; Brill 1992; Santopadre, Verità 2000; Towle *et al.* 2001; Angelini *et al.* 2002a, 2003, 2005a, 2005b, 2006b, 2010a, 2010b; Bellintani *et al.* 2006; Angelini 2009b), Switzerland (Henderson 1993), Germany (Hartman *et al.* 1997; Lorenz 2006), Bohemia (Venclová *et al.* 2011), Greece (Nikita, Henderson 2006), France (Guilaine *et al.* 1991; Gratuze 1999; Gratuze *et al.* 1998; Séguier *et al.* 2010; Croutsch *et al.* 2011; Plouin *et al.* 2012), Britain and Ireland (Raftery, Henderson 1987; Henderson 1988b; Paynter 2014).

Notably the early vitreous materials appear in Europe during the Early Bronze Age (EBA), and they are faience, not true glasses. This faience shows a LMHK composition and therefore they may be distinguished from the coeval Egyptian and Near Eastern productions. Moreover the high variability of the identified trace elements seems to suggest that since this early date there were different local production centres (Newton, Renfrew 1970; Harding, Warren 1971; Aspinall *et al.* 1972; Angelini *et al.* 2006a).

During the time spanning from the end of the EBA and the beginning of the FBA (Final Bronze Age) the story of the vitreous materials in Europe is still quite puzzling. Recent studies show that, depending on the specific age and geographic areas, both imported materials and local productions coexist (Angelini *et al.* 2002b, 2003, 2005a; Tite *et al.* 2005; Bellintani *et al.* 2005, 2006; Nikita, Henderson 2006; Varberg *et al.* 2015). Unfortunately the analyses on vitreous materials pertaining securely to this chronological range are still scarce and a global reconstruction of the development of glass pyrotechnology in Europe is extremely hard. Nevertheless in the last twenty years the number of archaeometric studies on BA vitreous materials has increased allowing, even if at the local scale, the reconstruction of their chemical and technological evolution through the different chronological phases of the Bronze Age (e.g. Plouin *et al.* 2012; Gratuze *et al.* 2013 for the Alsace-Lorraine area; Bellintani *et al.* 2006; Angelini 2011; Artioli, Angelini 2013 for Northern Italy).

Based on these considerations, the detailed archaeometric investigation of vitreous materials from well excavated and dated context, such as the ornaments discovered in the Tolochenaz VD - *La Caroline* necropolis, which is part of the *Boiron* necropolis, is very important. In the present work the analytical data of seven beads, six glasses and one glassy faience, will be presented and discussed in comparison with other Swiss and European ornaments that may be roughly dated to the same age.

MATERIALS AND METHODS

From the recent excavations in the Tolochenaz necropolis seven beads made of vitreous materials were discovered in two separate graves: the inhumation grave 1061 (6 beads), and the cremation grave 1089 (1 bead). In **fig. 1** the beads typologies, the inventory number of the finds, the data related to the excavations and the labels used in the present study are summarized. A detailed description of the archaeological context and of the associated grave goods may be found in chap. 4.4 in this volume. In figure 1 the main physical properties determined in the early phase of the study are also reported: dimensions (measured by a caliper), weight, and colors. The colors are described by means of the *Natural Color System* (NCS) tables, which may be easily converted in the *Munsell Color System* code.

The analysed beads belong to three typologies and are composed by glass with four different colours (**fig. 1-3**): three annular blue beads (**fig. 2,a-f**), one red annular bead (**fig. 2,g-h**), two barrel-shaped beads with spiral decorations (one with a blue body – **fig. 3,a-b** – and the other with a dark blue one – **fig. 3,c-d**), and one biconical pale blue bead (**fig. 3,e-f**).

1 Département de Géoscience, Université de Padova, Italie.

Label		Typology	Dimensions [mm]	Color / materials	NCS color code	Weight [g]	Classification data	Sampling area
Boi-AA		Annular bead	Dest= 5.8; Dint=3.0; H=2.5	Pale blue	S2555-B30G	0.064	T. 1061, N° inv. 26636-1	Glass bulge
Boi-AB1		Annular bead	Dest= 6.1; Dint=3.3; H=3.8	Blue	S3060-B20G	0.132	T. 1061, N° inv. 26636-3.3.2	Glass bulge
Boi-AB2		Annular bead	Dest= 5.1; Dint=2.7; H=3.5	Blue	S3060-B20G	0.070	T. 1061, N° inv. 26636-3.3.1	Glass bulge
Boi-BSpBBi	B	Fragment of a barrel shape bead with a spiral decoration	Dest= 9.0; Dint= 3.5; H= about 8.5; Tmax= about 3	Blue body	S8010-B10G	0.475	T. 1061, N° inv. 26636-4.2	Lateral fracture
	Bi			White spiral decoration	S3005-Y20R			Lateral fracture
Boi-BSpAzBi	Az	Half barrel shape bead with a spiral decoration	Dest= 7.3; Dint= 2.9; H=9.0-9.5	Pale blue body with a white spiral decoration	S2555-B40G	0.527	T. 1061, N° inv. 26636-2	From a chip close to the perforation
	Bi			White spiral decoration	S1500-N			From a chip close to the perforation
Boi-Bs		Biconical bead	Dest= 6.2; Dint= 1.8; H= 4.0	Pale blue	S1040-B50G	0.122	T. 1061, N° inv. 26636-3.5	Close to the perforation
Boi-AR		Annular bead	Dest= 6.5; Dint= 1.7-2.5; H= 2.0	Red surface, blue inner body	S2570-Y90R	0.060	T. 1089, N° inv. 26624-5	Close to the perforation

Fig. 1. Summary of the analysed vitreous ornaments listing the sampled areas, the bead typology, the physical parameters (weight, dimension, colour and NCS colour code –Natural Colour System), the grave code (T) and classification number (N° inv.). [Dest = external diameter of the bead; Dint= diameter of the hole; H = high].

The beads were studied in detail by Optical Microscopy (OM) with the purpose of characterizing the surface conservation state and to select the most appropriate area for sampling (reported in **fig. 1**). The instrument used is a stereo-microscope Nikon SMZ 645, equipped with a led circular Photonic Optics illumination and a Nikon Coolpix 6.1 digital camera, for the microphotography recording. Numerous photographs recorded at different focal planes were shot for each orientation of the beads; the stacks were then processed by the Helicon Focus 6.0 software (Helicon Soft ltd.) in order to create fully-focused 3D images. All the pictures in **fig. 2** and **fig. 3**, and all but two of the pictures in **fig. 4** are micro-3D images.

The annular blue beads are made of a semitransparent glass rich in bubbles (**fig. 2,a-f; 4,a**). The production mode of the beads may be inferred from the flow lines observed on the surface of the glass (**fig. 4,b**), and from the bulges present on one or both the sides of the beads (**fig. 2,b.g.f**). These evidences suggest that the beads were obtained by rolling a wire of hot glass on a bar, and no refinement of the shape was performed. This production mode is observed in other FBA annular beads from Northern Italy (Angelini 2009b; Angelini *et al.* 2010a).

On the other hand no glass bulges are visible on the red bead (**fig. 2,g-h**). The red color on the surface is very uniform and the black spots are actually due to incrustation of the soil that were not removed before of the consolidant application, so that the particles are now fixed upon the red surface (**fig. 4,c**).

The white glass wire of the barrel shaped beads decorations is well attached to the blue body, and the boundary between the two glass colors is irregular (**fig. 4,d-e**). These features indicate that the application of the decoration was carried out when both glasses (blue and white) were still hot, allowing a partial mixing (as verified by SEM-EDS analyses).

The biconical bead is totally opaque, and the surface shows black spots due to the soil incrustations (**fig. 3,e-f; 4,d**). By carefully monitoring the surface it appears gibbous, and in some areas small mineral grains are visible into or below the glass matrix (**fig. 4,d**).

The analyses were performed on micro-samples (ca. 200-500 μm^2) cut with a blade from the bodies and the decorations of the ornaments. The small chips were embedded in epoxy resin, polished and covered by a graphite layer to prepare them for the chemical investigation.

Textural and preliminary chemical analyses were obtained by a scanning electron microscope coupled with an energy dispersive spectrometer (EDS). The instru-

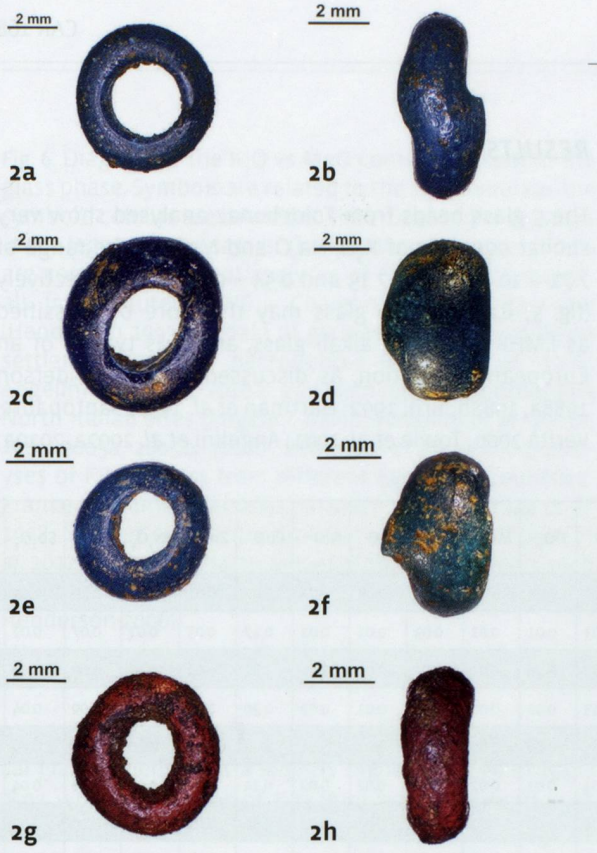

Fig. 2. The four analysed annular beads from Tolochenaz, as described in Table 1. Zenithal and lateral images of the beads with dimensional scales,: a)-b) Boi-AA; c)-d) Boi-AB1; e)-f) Boi-AB2; g)-h) Boi-AR.

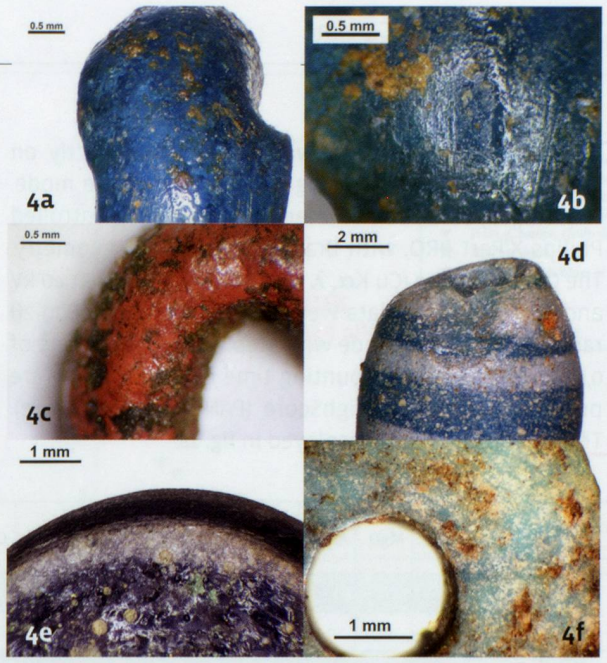

Fig. 4. Surface details of some beads recorded by a stereomicroscope (magnification 8-20 X), all but one (c) are 3D reconstructions. a) bead Boi-AA: detail of the well preserved and rough surface with evidence of bubbles and soil incrustations; b) bead Boi-AB2: in the centre flow lines due to the fabrication technique are present; c) bead Boi-AR: uniform red colour of the surface, with black spots due to soil incrustations fixed by the consolidant polymer; d) bead Boi-BSpAzBi: detail of a chipping where the contact between the blue and the white glass is visible; e) bead Boi-BSpBBi: irregular boundary at the contact between the blue and the white glass on the bead section; f) bead Boi-BS: rough surface of the biconical glassy faience. In some areas large quartz grains are visible below the glass.

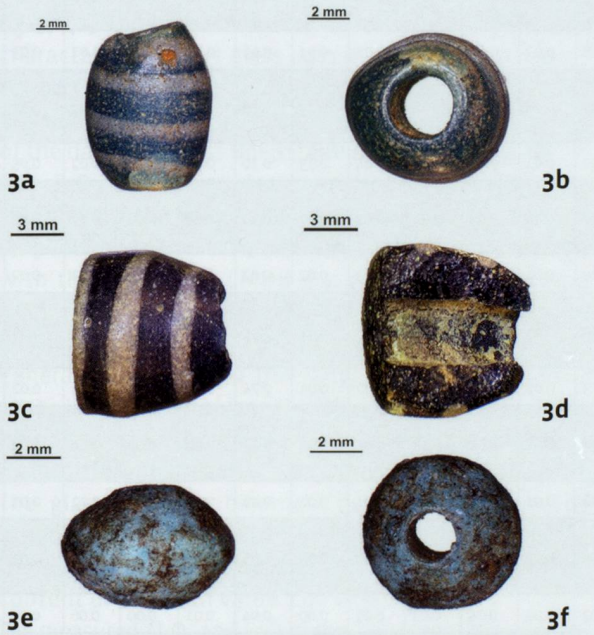

Fig. 3. The two barrel shaped beads with white spiral decoration and the biconical glassy faience from Tolochenaz investigated in the present study, as described in figure 1. Lateral and zenithal images of the beads with relative dimensional scales: a)-b) Boi-BSpAzBi; c)-d) Boi-BSpBBi; e)-f) Boi-BS.

ment used is a CamScan MX3000 equipped with a lanthanum hexaboride (LaB_6) electron source. The working conditions used are: accelerating potential of 20 kV, emission current of 70 μA, and working distance of 25 mm. The counting times applied during the EDS analyses is 60 s. A ZAF correction mode was used for the calculation of the chemical composition from the EDS measurements.

Quantitative chemical analyses were performed using a CAMECA SX50 electron microprobe (EPMA) fitted with four wavelength-dispersive spectrometers (WDS). The adopted instrumental conditions were: an accelerating voltage of 20 kV, a beam current intensity of 2nA for Na, K, Al, Si and of 20 nA for P, S, Cl, Ca, Ti, Mn, Fe, Co, Ni, Cu, Zn, As, Sn, Sb, Pb, and counting times of 5-10-5 s on background-peak-background, respectively. The spot size of the beam was about 1-2 μm, and the results were processed using the PAP (CAMECA) software for the ZAF corrections. The lowest detection limits were approximately 0.1 wt% for the major and minor elements, and they varied from 250 ppm for Co to 1400 ppm for Pb for trace elements. Figure 5 lists the EPMA chemical analyses of the glass phases expressed as oxides weight percent (wt%), calculated as a mean of 5÷10 points analysis, with the relative standard deviations (SD).

X-ray diffraction analyses were performed directly on the beads surface, operating in a non – invasive mode. The employed diffractometer is a computer-controlled Philips X'Pert PRO, with Bragg-Brentano θ- θ geometry. The Cu X-Ray tube (Cu $K\alpha_1$ λ =0.154056) operated at 40 kV and 40 mA, and the data were recorded in the 30-800 2θ range, in step scan mode with step width increments of 0,0170 2θ and a step counting time of 100 s. Data were processed by X'Pert HighScore (PANalytical software). The results are jointly displayed in **fig. 18**.

RESULTS

The 5 glass beads from Tolochenaz analysed show very similar contents of K_2O, Na_2O and MgO, in the range of 7.71 – 10.05; 6.04 – 7.15 and 0.54 – 0.88 wt% respectively (**fig. 5; 6,a; 7,a**). The glass may therefore be classified as LMHK, or mixed alkali glass, and it is typical of an European production, as discussed above (Henderson 1988a, 1988b; Brill 1992; Hartman *et al.* 1997; Santopadre, Verità 2000; Towle *et al.* 2001; Angelini *et al.* 2002a, 2010a;

Sample	Type of data	Na_2O	MgO	Al_2O_3	SiO_2	P_2O_5	SO_3	Cl	K_2O	CaO	TiO_2	MnO	FeO	CoO	NiO	CuO	ZnO	As_2O_3	SnO_2	Sb_2O_3	PbO	Total
Boi-AB1	Mean	6.26	0.71	2.13	73.96	0.09	0.04	0.15	10.06	1.25	0.09	0.01	0.66	0.00	0.02	3.97	0.02	0.00	0.36	0.09	0.01	99.88
	DS	0.14	0.02	0.15	0.55	0.03	0.01	0.01	0.36	0.03	0.01	0.01	0.03	0.01	0.02	0.17	0.03	0.01	0.07	0.02	0.02	
Boi-AB2	Mean	6.56	0.72	1.86	74.46	0.16	0.04	0.06	9.77	1.83	0.06	0.01	0.54	0.01	0.02	3.82	0.02	0.00	0.09	0.09	0.04	100.15
	DS	0.24	0.07	0.29	0.19	0.04	0.03	0.02	0.26	0.43	0.02	0.01	0.07	0.01	0.02	0.36	0.03	0.00	0.09	0.04	0.05	
Boi-AA	Mean	7.15	0.58	2.11	74.69	0.08	0.03	0.22	8.52	1.75	0.06	0.01	0.46	0.01	0.02	4.00	0.00	0.00	0.27	0.09	0.02	100.06
	DS	0.21	0.02	0.11	0.58	0.03	0.02	0.03	0.23	0.01	0.01	0.02	0.04	0.02	0.02	0.14	0.01	0.01	0.06	0.04	0.03	
Boi-AR	Mean	6.61	0.82	1.76	75.45	0.16	0.02	0.17	9.00	2.00	0.08	0.02	0.61	0.01	0.02	3.60	0.02	0.00	0.00	0.07	0.00	100.43
	DS	0.25	0.06	0.09	0.50	0.03	0.02	0.02	0.38	0.10	0.02	0.01	0.10	0.02	0.02	0.18	0.02	0.00	0.00	0.03	0.00	
Boi-BSp-BiAz	Az= Pale blue glass (mean)	6.88	0.54	1.67	76.47	0.07	0.04	0.06	9.62	1.54	0.05	0.01	0.49	0.01	0.02	2.25	0.02	0.00	0.01	0.12	0.02	99.88
	DS	0.21	0.03	0.11	0.57	0.02	0.03	0.01	0.24	0.13	0.01	0.01	0.05	0.01	0.02	0.09	0.02	0.00	0.01	0.04	0.04	
	Bi=White glass (mean)	6.58	0.68	1.85	74.77	0.10	0.05	0.07	9.35	5.75	0.07	0.02	0.53	0.01	0.00	0.31	0.01	0.00	0.02	0.12	0.08	100.36
	DS	0.24	0.04	0.10	0.24	0.03	0.04	0.02	0.09	0.16	0.02	0.02	0.02	0.01	0.01	0.03	0.01	0.00	0.01	0.03	0.06	
Boi-BSp-BBi	B=Blue glass (mean)	6.04	0.79	1.93	75.00	0.24	0.05	0.09	7.71	5.41	0.08	0.03	0.68	0.09	0.35	1.50	0.02	0.18	0.01	0.11	0.04	100.36
	DS	0.32	0.03	0.15	0.59	0.03	0.03	0.02	0.32	0.32	0.01	0.02	0.08	0.04	0.13	0.20	0.03	0.08	0.02	0.05	0.06	
	Bi=White glass (mean)	6.54	0.88	1.94	73.76	0.25	0.04	0.14	7.73	8.07	0.08	0.03	0.59	0.01	0.02	0.20	0.00	0.00	0.01	0.07	0.04	100.41
	DS	0.25	0.03	0.16	0.53	0.03	0.03	0.02	0.12	0.10	0.02	0.02	0.03	0.01	0.02	0.02	0.01	0.00	0.01	0.02	0.06	
Boi-BS	Glass rim (mean)	9.03	0.23	2.23	70.31	0.03	0.03	1.02	6.68	1.30	0.03	0.01	0.18	0.00	0.01	7.95	0.02	0.00	0.35	0.03	1.12	100.57
	DS	0.31	0.02	0.25	3.10	0.02	0.01	0.14	1.09	0.23	0.01	0.01	0.01	0.00	0.01	0.74	0.02	0.00	0.03	0.02	0.13	
	Glass IL (mean)	9.67	0.24	1.98	67.93	0.04	0.03	1.15	6.99	1.48	0.01	0.01	0.15	0.01	0.01	8.35	0.02	0.00	0.49	0.08	1.08	99.73
	DS	0.47	0.04	0.21	0.65	0.03	0.03	0.10	0.38	0.18	0.01	0.01	0.02	0.01	0.02	0.46	0.03	0.00	0.22	0.03	0.11	
	Glass core (mean)	8.20	0.32	2.52	71.27	0.05	0.06	1.05	6.54	1.78	0.02	0.05	0.18	0.00	0.00	6.63	0.01	0.00	0.56	0.03	1.02	100.29
	DS	0.32	0.02	0.37	0.12	0.05	0.06	0.01	0.10	0.03	0.01	0.04	0.03	0.00	0.00	0.04	0.01	0.00	0.06	0.05	0.09	
	Mean	8.97	0.26	2.24	69.84	0.04	0.04	1.07	6.73	1.52	0.02	0.02	0.17	0.00	0.01	7.64	0.02	0.00	0.47	0.05	1.07	100.29

Fig. 5. EPMA chemical analyses of the glass phase expressed as oxide wt%, determined as the mean of 5-10 point analyses. [DS = standard deviation of the measures; IL = interaction layer].

Fig. 6. Diagram of the K_2O vs MgO content present in the glass phase. Symbols are related to the sites, whereas the symbol's colours are related to the colour of the glass (as in the legends). The data of the Tolochenaz glasses (stars) are compared with: a) analyses of FBA vitreous materials from Hauterive NE – *Champréveyres*, Switzerland (Henderson 1993); b) data of glasses from the Frattesina settlement and its necropolises (Towle *et al.* 2001; Angelini *et al.* 2004, 2010a), and from numerous other FBA North Italian sites (Angelini 2009b; Angelini *et al.* 2002a, 2003, 2005a, 2005b, 2010b; Bellintani *et al.* 2006); c) analyses of FBA glasses from different European countries: France (Guilaine *et al.* 1991; Gratuze 1999; Gratuze *et al.* 1998; Séguier *et al.* 2010; Croutsch *et al.* 2011; Plouin *et al.* 2012), Germany (Hartmann *et al.*1997), Bohemia, Czech Republic (Venclová *et al.* 2011) and Elateia, Greece (Nikita, Henderson 2006).

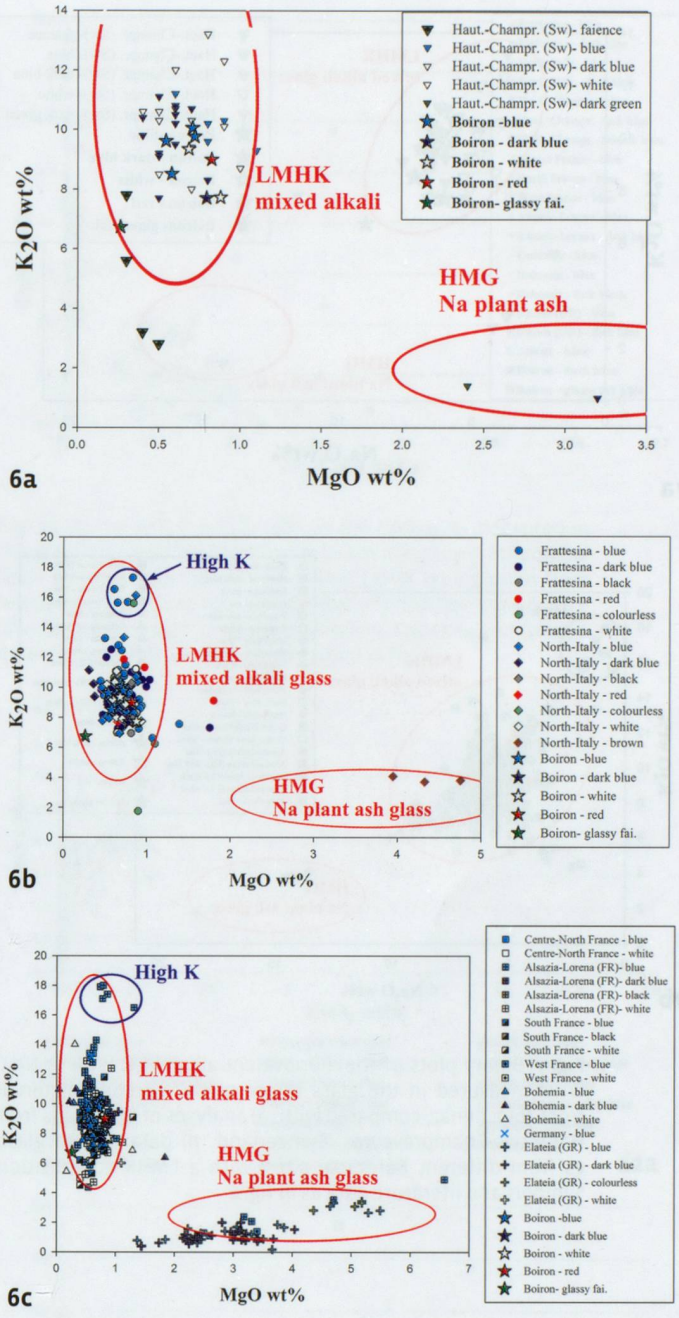

Bellintani *et al.* 2006; Artioli, Angelini 2013). The biconical glassy faience has a slightly higher amount of Na_2O (8.97 wt%), and lower of K_2O (6.73 wt%) and MgO (0.26 wt%), but the composition is in the observed range of the LMHK glasses.

As typical of the LMHK glasses the samples from Tolochenaz have a very low content of Ca (CaO = 1.25 – 2.00 wt%). Only the dark blue body of the barrel shaped bead Boi-BSpBBi and the two white glass decoration show higher Ca (CaO 5.41; 8.07 and 5.75 wt% respectively; **fig. 5; 7,a**). The high content of Ca in the white glasses is characteristic of this glass colour, and it is also related to the types of mineral inclusions present, but it is not unusual (see below); whereas the high Ca concentration of the dark blue glass Boi-BSpBBi-B is peculiar (**fig. 10**).

The P_2O_5 and Cl content are low in all the glass samples (in the range 0.07 – 0.25 and 0.06 – 0.22 wt% respectively). These values are perfectly compatible with those of other LMHK glasses (**fig. 8**, and relative data references). The very low content of P_2O_5 in LMHK glasses is reported in the literature and it is generally indicated in the range of 0.1-0.2 wt% (Brill 1992; Hartman *et al.* 1997), although differences may be observed in the glass compositions of ornaments from different areas, as discussed later on in detail. The glassy faience biconical bead differs from the other LMHK ornaments from Tolochenaz not only for the alkali concentration, but also for the rather high content of Cl (mean value 1.07 wt%; **fig. 5; 8**).

The measured Al_2O_3 and FeO of the Tolochenaz glasses plot in a very restricted area in the diagram of **fig. 9** (in the range 1.67-2.11 and 0.49-0.68 wt% respectively). No major differences in the content of these elements are observed between the four types of colored glass. Considering the high Al and the relatively low Fe amount present, we can assume that the same type of sand, quite devoid of Fe-bearing mineral, was used for the production of all the glasses.

The glassy faience Boi-BS has a high amount of Al_2O_3 (mean 2.24 wt%) comparable to that of glasses, but interestingly the Fe content is lower (FeO = 0.17 wt%) suggesting a careful selection of very pure sand for its production, or the addition of quartzite pebbles to sand.

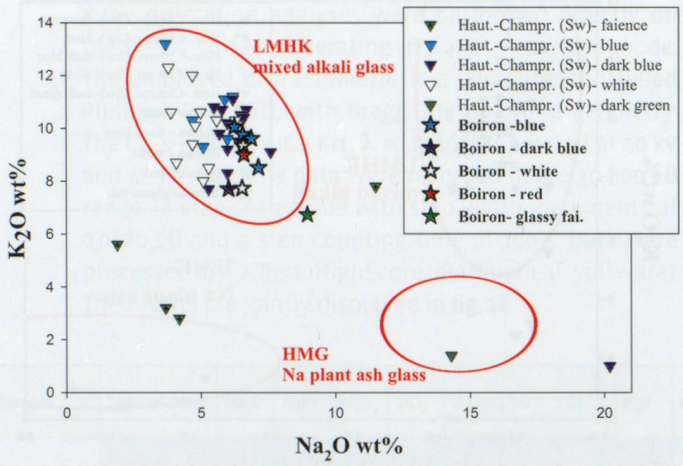

7a

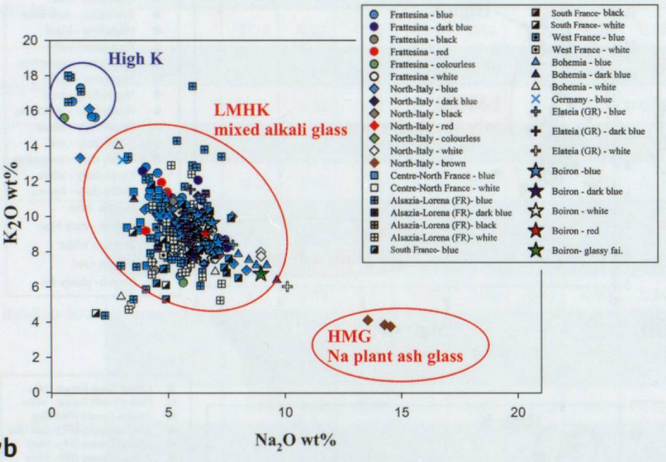

7b

Fig. 7. Binary plots of the monovalent alkali (K_2O wt% vs Na_2O wt%) measured in the glass phase of the vitreous materials from Tolochenaz, compared with: a) analyses of FBA beads from Hauterive-Champréveyres, Switzerland; b) data of FBA glasses from different European sites, with a LMHK composition. Symbols and literature data as in **fig. 6**.

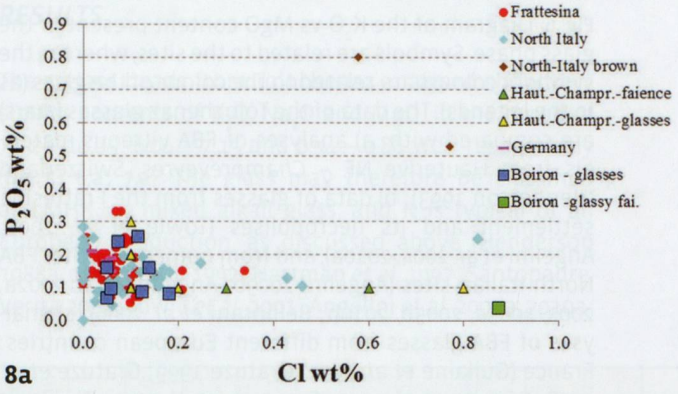

8a

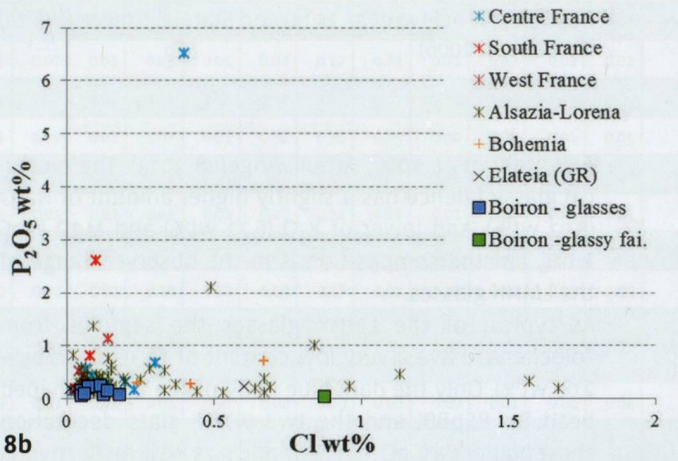

8b

Fig. 8. Diagrams of the P_2O_5 wt% vs Cl wt% content (enlarged in b) of the Tolochenaz beads compared with: a) Swiss, North Italian and German FBA glasses; b) LMHK glasses dated to the FBA from France, Bohemia (Czech Republic) and Greece. References literature data as described in **fig. 6**.

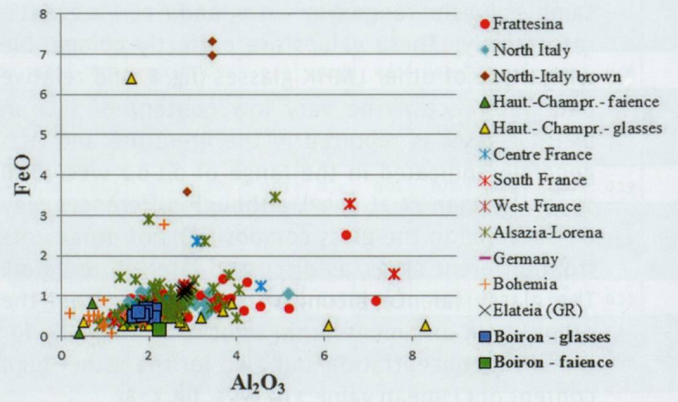

Fig. 9. Binary plot of the FeO wt% vs Al_2O_3 wt% measured in the glass phases of the vitreous materials ornaments from Tolochenaz, displayed together with other FBA beads from different European sites (from Greece and France only the LMHK glasses are plotted). References literature data as described in **fig. 6**.

THE BLUE GLASSES

The inner part of the red annular bead Boi-AR is composed by blue glass with a composition totally comparable to that of the other annular blue beads. The four annular beads and the barrel shaped one with a pale blue body (sample Boi-BSpAzBi) have been therefore plotted together as "*Boiron* blue glass" in the diagrams in **fig. 11-14**. These glasses are coloured by high amount of Cu (**fig. 11**): CuO = 3.60-4.00 wt% for the annular beads, and a little bit less for the barrel shaped bead (CuO = 2.25 wt%). The Cu is responsible of the intense pale blue of the glassy faience Boi-BS as well, and is present in extremely high quantity in the glass phase close to the rim of the bead, in the interaction layer (IL) and in the core, with a mean of CuO = 7.64 wt%.

The dark blue body of the barrel shaped bead Boi-BSpBBi also contains Cu (CuO= 1.50 wt%), but the dark shade is attributable to the presence of Co (CoO= 0.09 wt%, **fig. 11**).

The Cu is associated to traces of Sn in the glassy faience and in the three blue annular beads (SnO_2 = 0.09-0.47 wt%), whereas is absent in the red one and in the two barrel shaped beads (**fig. 12,b**). This means that both pure Cu and tin bronze were employed as colouring agents in the glass production. The CuO/SnO_2 ratio falls in the range of 11 - 43, which indicates the use of a bronze with about 2 - 8 wt% of Sn.

The Co-blue barrel shaped bead (Boi-BSpBBi) displays traces of Ni (NiO = 0.35) and As (As_2O_3 = 0.18 wt%) that are totally absent in the other samples. Similar characteristics are known in numerous different European Co-blue LMHK glasses, as discussed later (**fig. 13; 14,a**).

A peculiar chemical characteristic of the vitreous materials from Tolochenaz is that all the samples show traces of Sb (Sb_2O_3 = 0.05 – 0.12%, **fig. 14,b**).

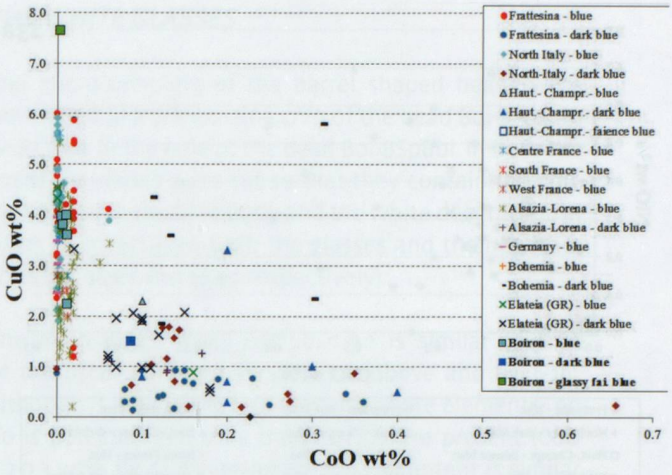

Fig. 11. In the plot the CuO wt% vs the CoO wt% measured in the glass phase of the Tolochenaz beads are shown for comparison purpose with the data of coeval LMHK blue glasses from North Italy, Hauterive NE – *Champréveyres* (Switzerland), France (divided by geographic regions), Germany, Bohemia and Greece. References literature data as described in **fig. 6**.

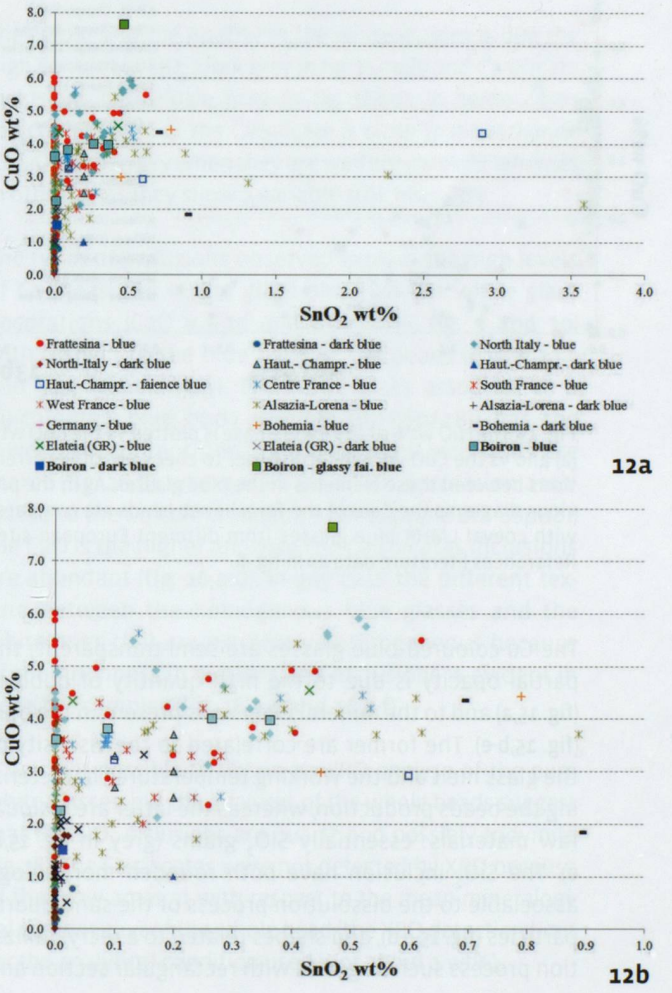

Fig. 12. Diagrams of the CuO wt% vs the SnO_2 wt% of the samples glass phase; in b) the first part of the plot a) is enlarged. The analyses of the Tolochenaz beads are displayed with the data of coeval LMHK blue glasses from different European sites as described in **fig. 6**. References literature data as described in **fig. 6**.

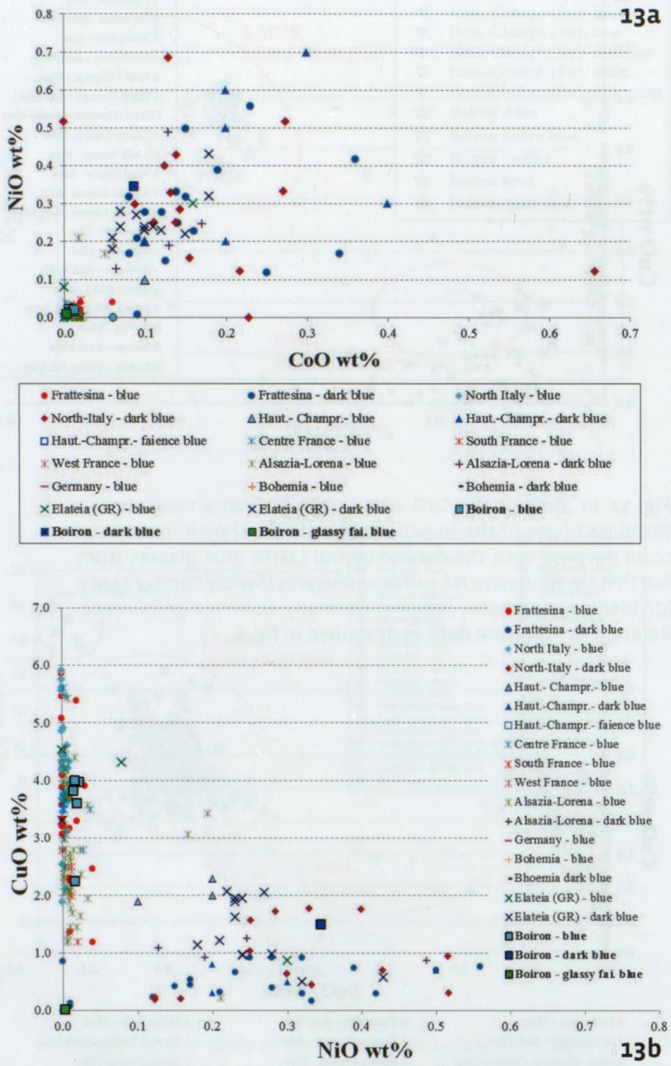

Fig. 13. The NiO wt% of the glass phase is plotted vs the CoO wt% (a) and vs the CuO wt% in (b), in order to check possible correlations between these elements in the blue glasses. As in the previous diagrams the data of the Tolochenaz beads are compared with coeval LMHK blue glasses from different European sites. References literature data as in **fig. 6**.

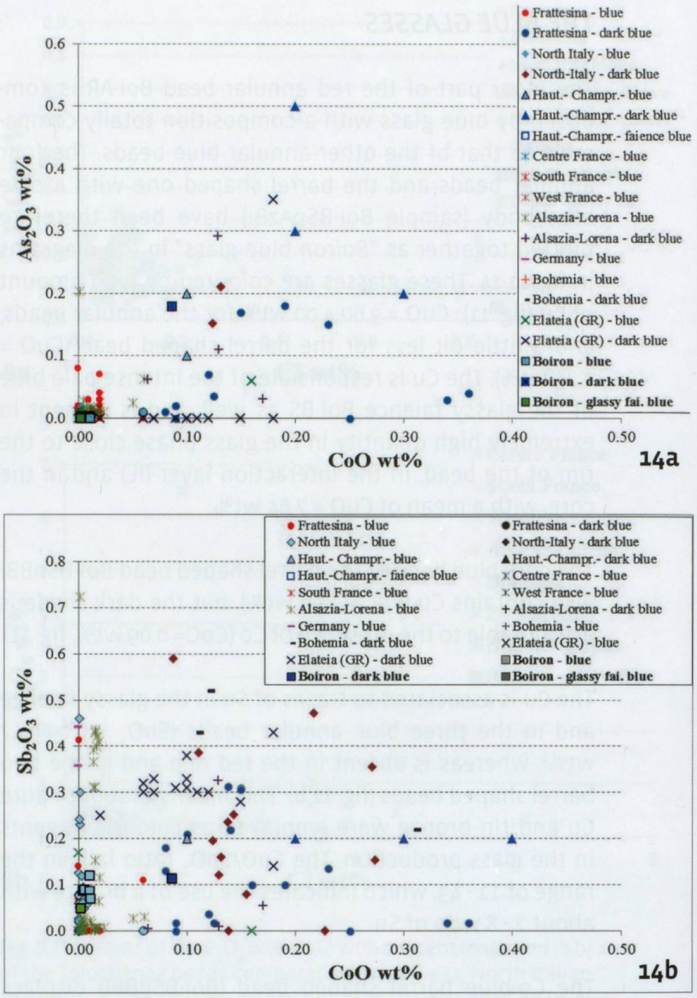

Fig. 14. CoO wt% of the glass phase in the Tolochenaz ornaments plotted with respect to: a) the As_2O_3 wt% content, and b) the Sb_2O_3 wt% content. Data of coeval LMHK blue glasses from various European sites are also reported. References literature data as described in **fig. 6**.

The Cu-coloured blue glasses are semi-transparent; the partial opacity is due to the high quantity of bubbles (**fig. 15,a**) and to the mineral inclusions present in the bulk (**fig. 15,b-e**). The former are correlated to the viscosity of the glass melt and the working temperature characterizing the beads production, whereas the latter are residual raw materials: essentially SiO_2 grains (grey in **fig. 15,b-e**). The SiO_2 inclusion have both rounded morphology associable to the dissolution process of the sand quartz particles (**fig. 15,c-d**), and shapes related to a recrystallization process such as grains with rectangular section and rarely dendrites (**fig. 15,e; 16,g**). The same features of SiO_2 inclusions are observed in the Co-coloured glass of the bead Boi-BSpBBi.

If the SiO_2 grains are large (70-80 microns or more) rounded thin fractures are visible in the glass matrix that surround the inclusion (**fig. 15,c**) and they may be associated to the volume contraction that happen during phase transitions in the production/working processes of the glass (Angelini *et al.* 2004; Artioli *et al.* 2008). Noteworthy, these fractures are weakness points, but also lines where corrosion processes

preferentially act enlarging the fracture, that in this case show also often a border of leached glass (dark border in the thick fractures in **fig. 15,d**). Normally the LMHK glasses are resistant to weathering and generally appear well preserved; this is the case of the Tolochenaz objects that exhibit only a thin layer (10-20 mm) of leached glass on the beads surface (dark grey in **fig. 15,f-h**).

The XRD analyses (**fig. 18**) show that in the blue annular beads Boi-AB1 and Boi-AB2 the SiO_2 inclusions are essentially quartz, whereas in Boi-AA tridymite is abundant as well.

The diffractograms of both the barrel shaped beads (the blue Boi-BSpAzBi and the dark blue Boi-BSpBBi) reveal that the glasses are rich in quartz and tridymite inclusions, and possibly present cristobalite traces. However we have to remember that the XRD analyses were performed in non-invasive mode on the whole surface of the objects, therefore in the case of the barrel shaped beads that have a white spiral decoration, the spectra display the mean mineralogical composition of the blue and the white glasses.

In addition the spectrum of Boi-BSpAzBi shows the presence of traces of calcite that are interpreted as a secondary deposition.

THE RED GLASS

The red annular bead Boi-AR is composed by a body of Cu-coloured blue glass that is exactly comparable to the other blue glasses (as discuss above). The superficial red colour of the bead is due to a uniform distribution of sub-micrometric Cu particles in a thin superficial layer (2-3 microns). The metal particles are clearly detectable by SEM (**fig. 15,h**), and even if is not possible to obtain a secure chemical analyses because of their small size, the EDS data show an extremely high content of Cu. However they are undoubtedly made of metallic copper, as revealed by the XRD analyses of the surface (**fig. 18**, brown spectrum: the third from the bottom).

The dark spots visible on Boi-AR are not related to the lack of the coloured surface or to weathering processes, but are associable to soil aggregates that were fixed by the consolidant during the restauration of the bead. This is supported by an OM study performed at high magnification (**fig. 4,c**) and confirmed by the SEM-EDS analyses (grey - dark grey aggregate in the upper-right part of **fig. 15,g**).

THE WHITE GLASSES

The micro-sampling of the barrel shaped beads were performed in a pre-existing chip of the bead Boi-BSpAzBi and close to the hole of the bead Boi-BSpBbi. In both the cases the slivers were cut so that they contain the contact between the blue body and the white decoration, in order to investigate both the glasses and their contact zone (**fig. 16,e-f and 16,a-c** respectively).

The main white glass composition is similar to that of the other coloured glasses (see above and **fig. 6-10**), although it essentially lacks chromophore elements: no Co is detected and only traces of Cu are present (CuO 0.2-0.3 wt%, **fig. 5**). Nevertheless the Fe content is similar to that present in blue glasses (fig 5, 9), suggesting that no special selection of the sand was made in order to produce white glasses. The use of sand is proved not only by the high Al content, but also by the remains of K-feldspar grains (with rounded boundaries) identified in both white glass samples.

The colour and the opacity in the white glasses is due the high content of SiO_2 (dark grey in **fig. 16,c-d,h**) and Ca-silicate inclusions (white-pale grey in **fig. 16,c-d**). In some cases the composition of the Ca-silicate is close to wollastonite ($CaSiO_3$), especially when they are well crystallised, whereas in other cases they show a variable stoichiometry.

The types of inclusions observed explain the high levels of Ca measured in the glass phase of the white glass decorations (CaO = 5.75 and 8.07 wt%, **fig. 5 and 10**) with respect to the blue body of the beads (CaO = 1.54 and 5.41 respectively). The white glass associate to a Cu-coloured blue body (sample Boi-BSpAzBi) has the lower CaO content and the Ca-silicates inclusions are scarce (**fig. 16,h**), whereas in the white decoration associated to the Co-coloured blue body (sample Boi-BSpBBi) the CaO is the higher and also the Ca-silicates inclusions are abundant (**fig. 16,a-d**). In any case the different texture between the homogenous blue glasses and the white ones that are extremely heterogeneous because of their richness in bubbles and inclusions is evident in both the samples (**fig. 16,a-c and 16,e-f**).

It was not possible to obtain an XRD analyse of the pure white glasses, but the analyses of the whole beads suggest that the SiO_2 inclusions are quartz and possibly tridymite (**fig. 18**). The Ca-silicates were not detected by XRD because of their low amount with respect to the mean mineralogical composition of the whole bead (the XRD detection limit for the analytical condition used is of about 1 wt%).

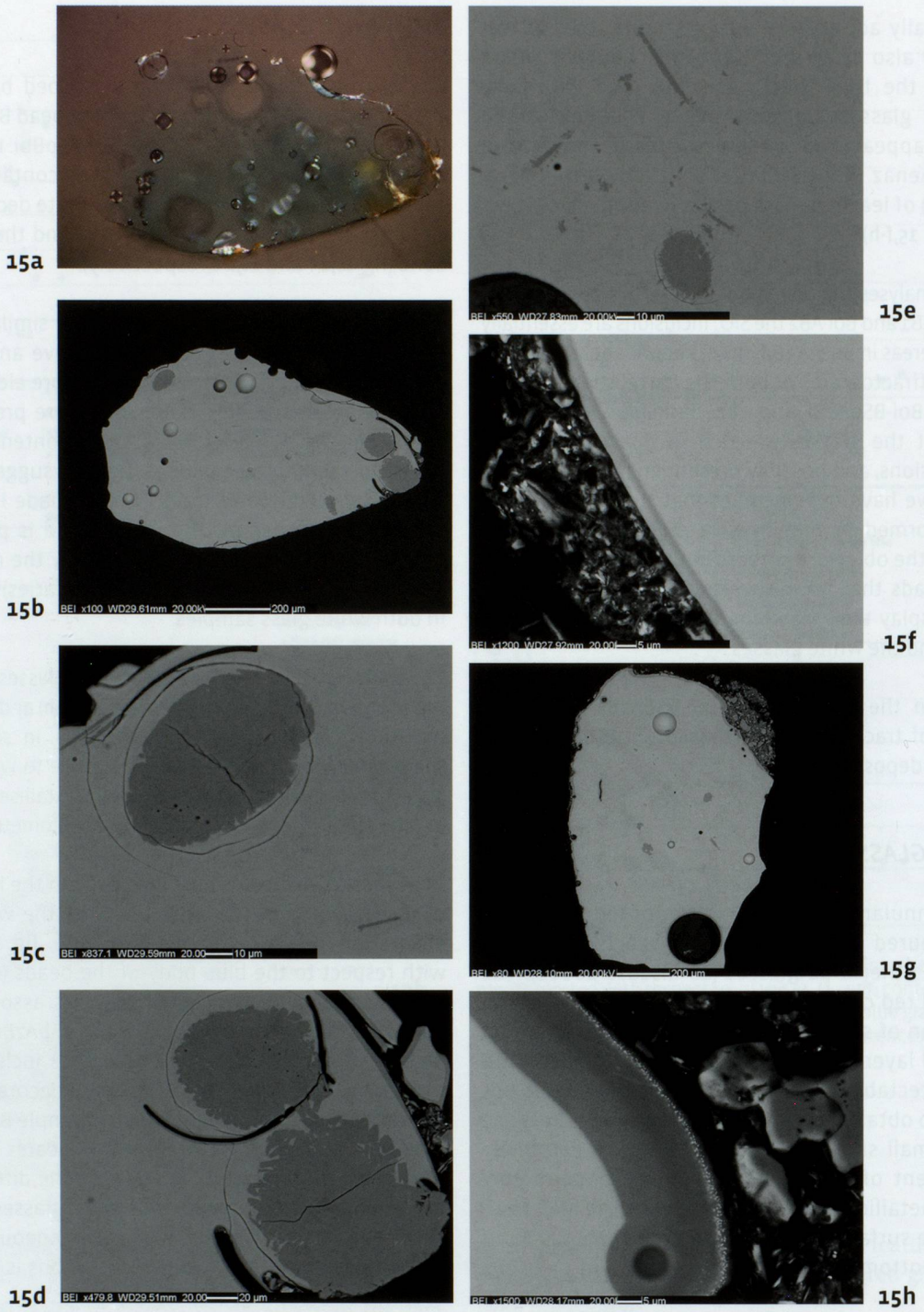

Fig. 15. OM microphotography (a - magnification 20X) and SEM-BSE images (b-h) of the four annular beads from Tolochenaz, respectively samples: a)-d) Boi-AA. In a) the high amount of bubbles throughout the transparent blue glass is visible; b) homogeneous glass phase with large rounded inclusions of SiO_2 (grey); c) fractures surrounding a large SiO_2 g.ain due to the phase transitions that occur during the glass production/cooling; d) large round fractures that surround the SiO_2 grains, due to the weathering process; e)-f) sample Boi-AB2 that show homogeneous glass phase with large SiO_2 inclusions, with both rounded and rectangular sections (e); in f) the surface of the beads show incrustation of soil (left) and a thin layer (2-3 microns) of weathered glass (dark grey); g)-h) Boi-AR. The red bead show a texture of the inner part similar to the one of blue glasses [g], but on the surface sub-micrometrics particles of metallic Cu (white) are widespread (h).

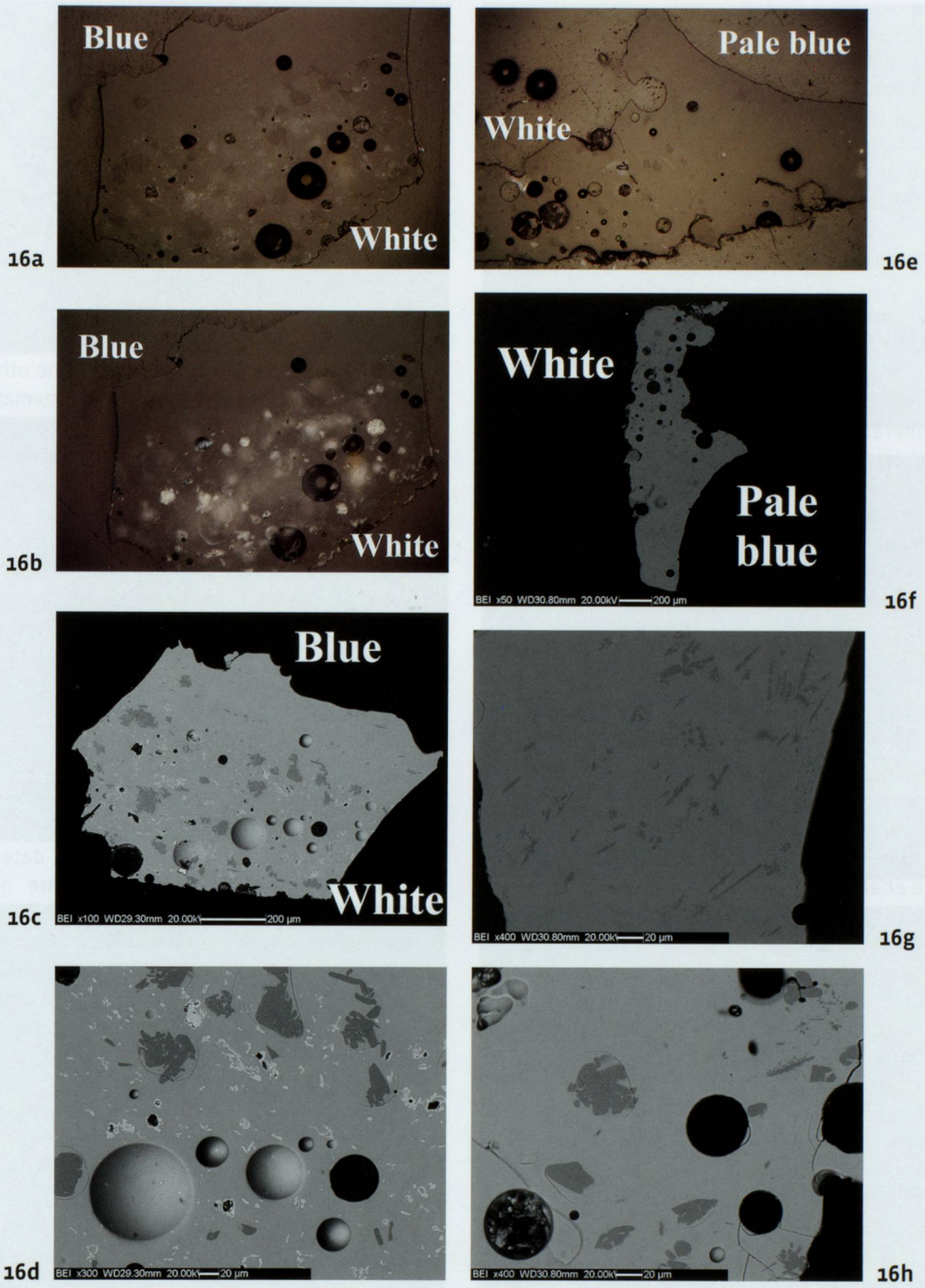

Fig. 16. OM microphotographs recorded in reflected light (a, b and e – magnification 20X) and SEM-BSE images (c, d, and f-h) of the two barrels shaped beads with spiral decoration from Tolochenaz. Respectively samples: a-d) Boi-BSpBBi, and e-f) Boi-BSpAzBi. The OM images a-b of Boi-BSpBBi, recorded with cross Nicols in b), show the different texture of the homogeneous blue glass with respect to the heterogeneous white glass, rich of inclusions and bubbles. The inclusions in the white glass are due to SiO_2 grains (dark grey in c-d), and Ca-silicate with variable stoichiometry, in some case close to wollastonite (white in c-d). Also the pale blue and white glasses of the bead Boi-BSpAzBi display similar differences in the texture (e-f), but in this case the SiO_2 grains in the pale blue glass are small and with rectangular section [g], whereas the white glass is essentially rich only in SiO_2 large inclusions and bubbles (h), even if rare Ca-silicates and K-feldspar are present.

The contact between the blue and the white glass is continuous (**fig. 4,d-e; 16,a-c; 16,e-f**). Profile EDS analyses in the contact area show a diffusion zone with a glass matrix composition that is a mean between blue and white glass (particularly evident for the Ca content). It is possible to deduce that the white decorations were applied at quite high temperature when the blue beads were still hot, allowing a very good adhesions and diffusion of the two glasses.

THE GLASSY FAIENCE

The biconical bead Boi-BS is composed by similar quantity of mineral and glass phases, and may be defined as glassy faience (Angelini *et al.* 2002b; Bellintani *et al.* 2006; Artioli *et al.* 2008; Artioli, Angelini 2013), actually the sample is highly vitrified, as evident by the OM image reported in figure 17,a. No glaze is present (**fig. 17,b-c**), and SiO_2 grains are visible also in the surface layer of the bead. The interaction layer (IL) is thick and continuous, hardly distinguishable from the core. It was impossible to cut a section of the bead and therefore the real texture of the inside is unknown, but as a first approximation we can assume that the inner part of the cut sample is similar to the core structure. This portion of the sample is porous and it contains indeed a high portion of glass phase (**fig. 17,f**). These features suggest that the bead was produced by the efflorescence glazing technique (Tite, Bimson 1986; Tite *et al.* 2008). On the other hand by observing the chemical variations of the glass phase from the rim to the core of the bead (**fig. 5**), and also taking into account a possible light weathering of the glass on the surface, there is an increase in Mg and Ca, and a consistent concomitant decrease in Na, K, and Cu. In case of the efflorescence technique, Tite *et al.* (2008) report a Na enrichment and a K, Ca, Mg and especially Cu depletion of the surface interparticles glass of the faience with respect to the glass in the core. The chemical profile recorded in Boi-BS does not fit perfectly with this description because of the higher contents of K and Cu on the external part of the sample. A possible hypothesis is that the efflorescence glazing method was used, combined with a direct application on the surface of a mixture rich in alkali and coloring agents. The bead was then fired after a very short drying period, because no glaze is formed on the surface.

The mineralogical analyses of the glassy faience performed by XRD show that quartz is the main phase, moreover there are traces of K-feldspar (identified also by SEM-EDS, pale grey grains in **fig. 17,d-e**) and of secondary calcite. The SiO_2 inclusions are variable in size from a few microns up to 80-100 mm. The small quartz grains exhibit rounded rim, suggesting a partial dissolution, whereas the larger grains are often angular in shape.
Numerous SnO_2 inclusions are observed in the overall sample, from the rim to the core (white in the BSE images, **fig. 17,b-f**). Sn traces are measured also in the glass phase (mean SnO_2 = 0.47wt%), with a CuO/SnO_2 ratio of 16.3, corresponding to a bronze with 5.7 wt% of Sn.

The glass phase of the Boi-BS glassy faience has an LMHK composition, comparable with those of the other LMHK glasses from the same site. But small and systematic chemical differences are present with respect to the glass beads (see **fig. 5** and previous discussion). Moreover the glass phase contains lead (mean PbO = 1.07 wt%), never detected in the other samples. These chemical variations point to the adoption of similar recipes for the glasses and glassy faience productions, but implying the use of different or differently treated raw materials. Specifically, the higher content of Na and Cl in the glassy faience and the lower K suggests a different composition of the plant ash used, whereas the higher amount of Cu, Sn and Pb are related to the addition of higher quantity of metals.

DISCUSSION

Despite the fact that the glass beads dated to the BA discovered in Switzerland are quite numerous (chap. 4.7.3), to date analytical investigations have been performed only on the ornaments from Hauterive NE – *Champréveyres* (Henderson 1993). The vitreous materials from Hauterive NE – *Champréveyres* have typologies and age comparable with ones of the beads from Tolochenaz, actually they are annular, barrel shaped, and horned eyed beads dated to 1050-1030 BC (Rychner-Faraggi 1993). These data are reported in the diagrams in **fig. 6-14**.

The comparison has been extended to other coeval European glasses for which analytical data are available, in particular focusing the attention on materials from the close geographic areas (France, North Italy and Germany). In the plots reported in **fig. 6-14**, are displayed data from the following contests:

1- Frattesina (Rovigo), Veneto region in North-Eastern Italy: To date the Frattesina settlement and the very close site of Mariconda di Melara (Rovigo), are the only two BA contexts with secure evidence of glass production: scraps of raw glass, crucibles, glass wastes

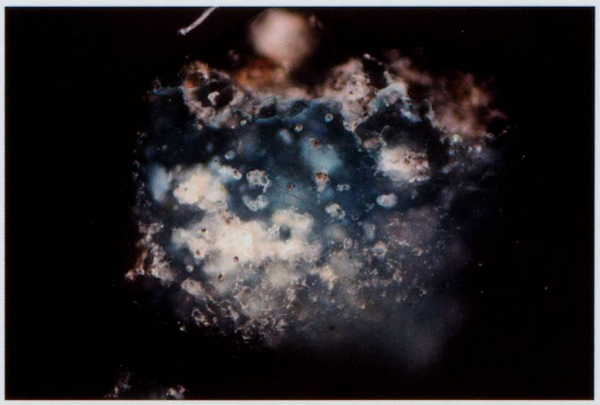

17a

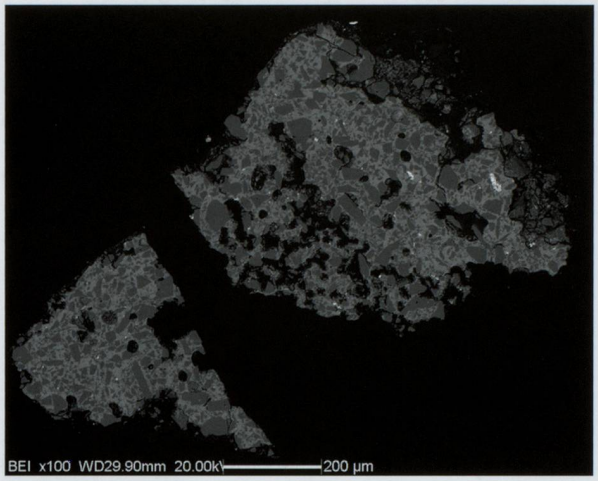

17b

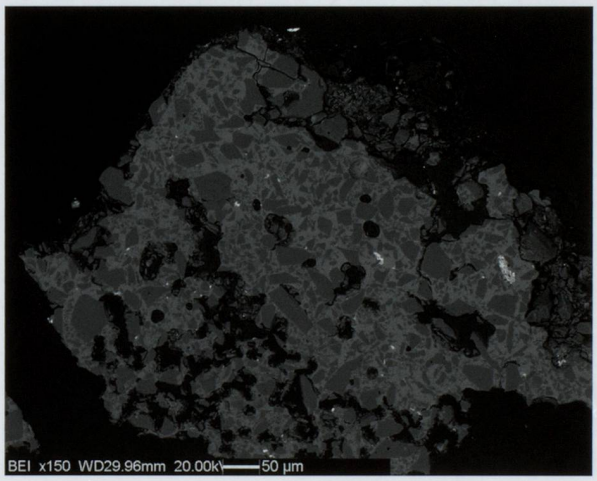

17c

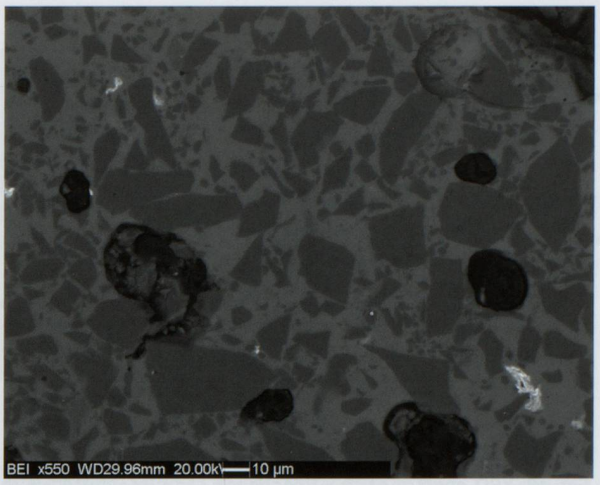

17d

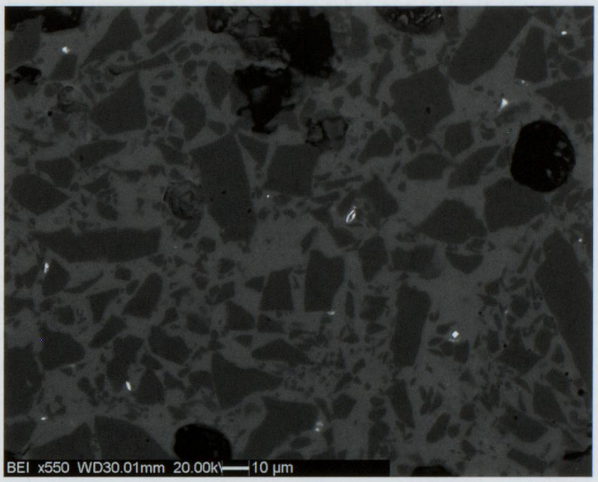

17e

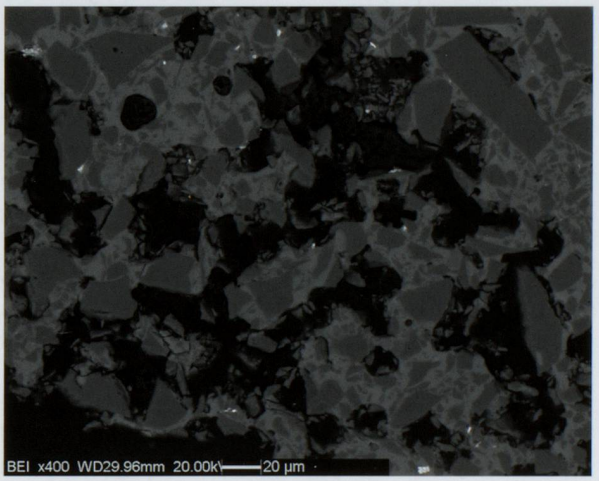

17f

Fig. 17. OM microphotography (a - magnification 20X) and SEM-BSE images (b-f) of the biconical blue bead Boi-BS. In a) and b) is visible the general texture of the samples: no glaze layer is present, whereas the interaction layer (IL) is thick and continuous, merging to the core with no clear boundary. d)-e): the IL is rich in SiO_2 grains (dark grey), SnO_2 inclusions (white) and show the presence of several K-feldspar (pale grey). The inner part of the sample (f), that we can suppose similar to the core of the bead, is more porous and with large amount of interparticles glass.

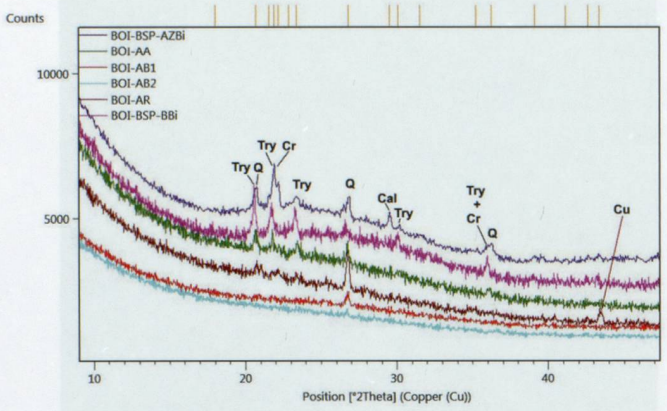

Fig. 18. XRD spectra of the Tolochenaz samples, shifted with respect to the Y axe in order to permit the comparison (the relative intensity of the diffractograms are not in scale). [Try = tridymite; Q = quartz; Cr = cristobalite; Cal = calcite; Cu = copper].

and plates with glass incrustations. Numerous glass ornaments were also unearthed in the two necropolis of Frattesina: Fondo Zanotti and Narde. The beads, dated to the Italian FBA, are mainly annular (about 2700 beads), but numerous other typologies are also present, included the barrel shaped and the horned eyed beads (Bietti Sestieri 1996; Bellintani *et al.* 2006; Bellintani, Stefan 2009 and references quoted therein). The glasses from these contexts were analysed by several authors, however in order to simplify the diagrams only a representative selection of data from the Frattesina settlements and necropolis, and from Mariconda di Melara are plotted (data from Towle *et al.* 2001; Angelini *et al.* 2004 and 2010a). The other available analyses not reported here are totally comparable (as demonstrated in Angelini *et al.* 2010a) and may be found in: Biavati 1983; Henderson 1988a; Brill 1992; Santopadre, Verità 2000.

In the Veneto region other three sites where scraps of raw glass were found are known: Montagnana (Padova), Fondo Paviani (Verona) (Cupitò *et al.* 2015) and possibly Caorle (Venice) (Bellintani *et al.* 2006).

2 - Northern Italy: In this area glasses dated to the FBA were discovered in numerous sites, and recently several archaeometric investigation were performed. The available data of these materials are plotted together, without details on the specific proveniences that may be found in the relative bibliography (data in: Angelini 2009b; Angelini *et al.* 2002a, 2003, 2005a, 2005b, 2010b; Bellintani *et al.* 2006).

3 - France: A huge amount of chemical data on BA vitreous materials from France are available in the literatures thanks to the work of Bernard Gratuze and his co-workers. In the present paper a large selection of data related only to materials dated to the BFIIa-BFIIIa are considered in detail. This chronological range was chosen because it roughly matches the age of Italian FBA glasses, and it is also suitable for the comparison with the beads from *Boiron*. Based on the beads proveniences the data are divided in four macro-areas: West, Centre, and South France, and Alsace – Lorraine. The data reported in the diagram for comparison are from: Guilaine *et al.* 1991; Gratuze 1999; Gratuze *et al.* 1998; Séguier *et al.* 2010; Croutsch *et al.* 2011; Plouin *et al.* 2012.

4 - Germany: In the diagrams are reported the data of annular beads from the sites of Borken-Kleinenglis (Schwalm-Eder-Kr.) and Lohfelden – Vollmarshausen (Kr. Kassel) dated to the 12th – 8th century BC (Hartman *et al.* 1997). Also a large set of *analytical* data is available for glass beads from the hoard of Stadtallendorf (Kr. Marburg-Biedenkopf) (Lorenz 2006). Some of the ornaments are tentatively dated to the FBA, but mainly on the bases of their typologies and chemistry, therefore we prefer to omit these results from the detailed comparison in the plots.

5 - Czech Republic: A set of annular, barrel shaped and eyed beads dated to the HaA (12th- early 11th century BC) from four Bohemian sites were recently analysed by Venclová *et al.* (2011). All these data are reported in the plots.

6 - Greece: A detailed analytical study of the vitreous materials from the necropolis of Elateia (Phokis) was performed by Nikita and Henderson (2006). The results show the presence of a large group of LMHK glasses, that are roughly coeval with the other LMHK European productions. The vitreous ornaments from Elateia belonging to the LH IIIA-Submycenaean chronological range were considered in the plots here presented. These objects are beads and decorated plaques, but the glass that show LMHK composition are only annular, horned eyed and segmented beads.

Based on the K, Na, Mg and Ca contents (**fig. 6, 7, 10**), all but two of the vitreous materials from Hauterive NE – *Champréveyres* result with LMHK composition, whereas two have an HMG recipe. The same is true for the North Italian glasses, whereas the samples from Frattesina, Germany and Bohemia, such as the *Boiron* beads, are only LMHK glasses. The two HMG glasses from Italy are brown (HMBG), with high Fe, Ca and Al, and with abun-

dant inclusions of diopside, augite and Cu sulphides. The HMBG glasses are present in North Italy since the Middle Bronze Age 3-Recent Bronze Age (about 1450-1200 BC) and since they are not found out of Italy, they are considered local production (Angelini *et al.* 2005 a or b; Bellintani *et al.* 2006; Angelini 2011; Artioli, Angelini 2013). Interestingly one of the HGM from Hauterive NE – *Champréveyres* described as dark green, show similar high level of Ca and Fe (**fig. 6,a-b and 10,a**), but unfortunately no information are reported about its mineralogy and texture. No similar glasses are present in the Tolochenaz necropolis.

The French glasses are mainly of the LMHK type, but several HMG glasses were identified in the West (at Rancogne, Gratuze *et al.* 1998) and in Alsace – Lorraine (Plouin *et al.* 2012; Gratuze *et al.* 2013). On the contrary the majority of the glass from Elateia are HMG, and only 18 are LMHK.

Within the Italian FBA materials there is a sub-group of glasses rich in K and poor in Na (Angelini *et al.* 2004, 2010a; Bellintani *et al.* 2006; Towle *et al.* 2001). This compositional class differs from the Middle Age K-rich glasses because of the low levels of Ca and Mg, that are similar to the ones of the other LMHK glasses (**fig. 6,b and 7,b**). This peculiar composition was identified also in a bead from Clanezzo (Bergamo, North Italy) (Angelini *et al.* 2010a), and in several samples from Alsace – Lorraine (Plouin *et al.* 2012; Gratuze *et al.* 2013). To date the K rich LMHK recipe is known only from France and North Italy, suggesting the existence of production that use a different alkali source with respect to the classic LMHK glasses.

The very low content of P_2O_5 in the LMHK glasses (**fig. 8**) is well known in the literature and is generally indicated in the range of 0.1-0.2 wt% (Brill 1992; Hartman *et al.* 1997), even if the more recent high number of analyses performed on French glasses have shown that numerous LMHK glasses may have P_2O_5 up to 1%, or more (Guilaine *et al.* 1991; Gratuze 1999; Gratuze *et al.* 1998; Séguier *et al.* 2010; Plouin *et al.* 2012). The Cl content is also very low in the LMHK glasses, generally below 0.2 wt%, but some samples from North Italy and especially numerous beads from France have a higher Cl content, up to 1 wt% or even more (**fig. 8** and related data references). The P and Cl contents are related to the type of flux used and to their treatment. Actually it is known that HMG glasses, obtained by the use of sodium plant ash as flux, exhibit a generally high amount of Cl (normally in the range 0.5-1wt%) and variable but usually high P_2O_5 (approximatively in the range of 0.3-1 wt%) (Hartman *et al.* 1997, and data in Brill 1999; Nikita, Henderson 2006; Angelini *et al.* 2002a, 2003, 2005a). The two FBA Italian brown glasses (**fig. 8,a**) clearly plot in a separate area with respect to the FBA LMHK beads, and they are considered HMG glasses (Angelini *et al.* 2005a). The dark green glass from Hauterive NE – *Champréveyres* that has an HMG recipe is not reported in figure 8, because the P amounts was not measured, but the Cl content is coherently very high (0.9 wt%, Henderson 1993).

The LMG glasses, that are produced using natron as flux, show only trace of P and high Cl contents (about 1% and higher, Hartman *et al.* 1997).

In **fig. 8**, we can observe that the glasses from Tolochenaz are perfectly comparable in the P and Cl contents with the finds from Hauterive NE – *Champréveyres* and from the North Italian production, and also with the majority of the other European LMHK materials. However generally the French glasses differ for the higher contents of one or both these elements. It is also notable that the LMHK faience from Hauterive NE – *Champréveyres* are characterised by higher amount of Cl with respect to the glasses, similarly to the glassy faience and glasses from Tolochenaz.

The content of Al in the LMHK glass is variable (**fig. 9**), but generally high enough to suggest the use of sand as source of quartz, as noted in numerous archaeometric studies of the FBA glasses. Generally Al_2O_3 is less than 3.5 wt%, but it has been measured up to the 8 wt%. Considering the specific characteristics of the objects with high Al, no correlations between typology, colour and chemical composition is observed.

Except for the HMG glasses from North Italy and Hauterive NE – *Champréveyres* discussed above, the LMHK FBA glasses generally display a FeO amount minor than 1.5 wt%, and only in a few cases is in the range of 1.5-2.0 wt%. Normally the higher FeO content correspond to a very dark blue – black colour of the glass. The Al and FeO levels of the samples from Tolochenaz fit perfectly in the field of the LMHK glasses with mean Al and low Fe contents.

The texture and the mineralogical composition of the glasses have been studied only in a few works, since in the majority of the cases only the chemistry is investigated. The types of inclusion observed in the glasses may be roughly divided in three classes: 1) inclusions related to the colouring agents: metal particles, metal oxides and sulphides, opacifier, etc.; 2) residual grains of the silica sources (i.e. sand or quartz pebbles); 3) devitrification crystals.

The results of the analyses show that the inclusions of the class 2) and 3) are abundant in all the samples from Tolochenaz (see above discussion). The same types of SiO_2 inclusions, their specific morphology, and the general texture of the glasses from Tolochenaz, are reported also in FBA glasses from Frattesina (Santopadre, Verità 2000; Angelini *et al.* 2004 and 2010a), as well as in other coeval North Italian beads (Angelini *at al.* 2005a and 2010b; Angelini 2009b; Artioli *et al.* 2008; Artioli, Angelini 2013). These features may be considered characteristic of the LMHK European production, and they are not present in the HMG and LMG glasses that normally are homogeneous.

COLOUR OF THE GLASSES

The diagrams reported in **fig. 11-14** report the data of blue coloured glasses, faience and glassy faience from the considered contexts that have LMHK composition, in order to compare the chromophore elements contents and the trace elements.

The majority of the glasses are coloured by Cu, that is generally present in the range of CuO = 1-6 wt%, interestingly the glassy faience from Tolochenaz shows the highest amount of Cu. Traces of Sn are observed in some of the Cu-blue glasses (**fig. 12**), whereas other contain only Cu. It is known that in the Frattesina production and more generally in the FBA LMHK glasses, both pure Cu and tin bronze were use as colouring agents (Gratuze *et al.* 1998, 2013; Towle *et al.* 2001; Angelini *et al.* 2002a, 2006b, and 2010a, Angelini 2009b; Artioli, Angelini 2013; Plouin *et al.* 2012). In the majority of the analysed beads from Hauterive NE – *Champréveyres* the Sn was not measured, but in the few samples from which data are available the Sn is present in trace amounts (SnO_2 = 0.1-0.2 wt%). In the beads from Tolochenaz the Sn is present only in the annular pale blue beads, whereas is absent in the barrel shaped pale blue beads and in the inner blue glass of the red bead. However the glasses from the other sites do not show the same correlation between typologies and composition.

The dark blue glasses are coloured by Co, but Cu is also invariably present. In the majority of the Co-coloured beads the CuO is less than 1%, but the Greek beads, some glasses from North Italy and from Hauterive NE – *Champréveyres*, and the dark blue bead from Tolochenaz have CuO in the range of 1-2.5 wt%. Based on the high CuO/CoO ratio, and on the high content of Fe and Ni, Nikita and Henderson (2006) suggest a possible local production of the LMHK Greek glasses. Anyway considering the large dataset of LMHK glasses here discussed, it is possible to note a variable content of Ni and the Greek beads do not seem to show a peculiar concentration of this element. The same is true for the Fe contents (**fig. 9**). Instead the high CuO/CoO ratio is specific to Greek and few other samples, including the blue Boi-BSp-BBi sample. Moreover a correlation between the Co and the Ni contents is present (**fig. 13,a**).

The Co is associated also to As trace (**fig. 14**), and the systematic association of Co-Ni-As is considered typical of the European LMHK glasses (Towle *et al.* 2001; Angelini 2004, 2010a; Artioli, Angelini 2013; Plouin *et al.* 2012). The source of Co is unknown and strongly debated in the literature, but based on the chemistry of the glass it is clear that it is different from the Egyptian and Near Eastern sources. A further differentiation may be obtained if the Sb content- is measured. As shown in figure 100,b traces of Sb are present in the Swiss glasses (both from Tolochenaz and from Hauterive NE – *Champréveyres*), and in some objects from Italy and Alsace – Lorraine, whereas it is absent in all but one of the Greek beads.

Red glass is rare in Europe during the BA: it appears only in the FBA in the Frattesina production where a large number of annular beads and numerous scraps of glasses with a surface uniformly red were discovered. The red colour was obtained applying reducing conditions to Cu-blue coloured glass, to create metallic Cu particles in the material. The red colour is not due to the formation of cuprite as initially supposed (Brill 1992; Santopadre, Verità 2000), but to sub-micrometric particles of metallic Cu as demonstrated by XPS, TEM and XRD analyses (Angelini *et al.* 2004).

The red bead from Tolochenaz is coloured in the same way. In principle, it is also possible that the fire during the cremation may reduce the Cu of blue beads, but as it is generally observed in other sites, the resulting colour is not uniform and the glass often shows evidence of a second firing. Therefore, based on the characteristics described above, we believe that this hypothesis may be excluded for the Tolochenaz red bead. To our knowledge annular red beads in FBA have been reported only from Frattesina and from Fondo Paviani (Italy) (Cupitò, Angelini *in press*).

Chemical and mineralogical studies on FBA white glasses from North Italy (Angelini *et al.* 2002a, 2005b and 2010a) show that two types of white glass were in use:

type 1: the chemical composition is comparable to that of the other LMHK glasses with the exception of a higher content of Ca, which in the glass phase was mea-

sured in the range CaO = 6-11 wt%. The glass is rich in inclusions of SiO_2 and Ca-Silicates forming about the 8% in volume of the glasses. Ca-silicates are both crystalline and amorphous;

type 2: glass with a chemical composition totally comparable with the LMHK glass (the CaO is measured in the range of 1.4-2.1 wt%). The glass is very rich in SiO_2 inclusions amounting to about the 18% in volume of the glasses.

As reported in **fig. 10,c** several analyses are available for FBA white glasses from France, Greece, Bohemia and from Hauterive NE – *Champréveyres* (references as in **fig. 6**), although these materials are generally characterized only from a chemical point of view, therefore it is not possible to know the type of mineral inclusions present in the glass. Henderson (1993) reports the presence of tridymite in 2 white samples (XRD analyses) and he notes the high Ca levels of the white glasses. Also Gratuze often reports the presence of high Ca in white glasses, and he justifies it with the possible presence of wollastonite (Gratuze *et al.* 1998; Croutsch *et al.* 2011; Plouin *et al.* 2012; Gratuze *et al.* 2013). Actually, the measurement of the Ca amounts may help in the identification of the type of white glass, as visible in **fig. 10,c**: white glass with relatively low Ca (type 2) are present in a very few samples from Hauterive NE – *Champréveyres* and from France, but the majority of the materials have high Ca (type 1). Both the white decorations from the Tolochenaz barrel shaped beads are of type 2 white glass.

CONCLUSIONS

The archaeometric study of the vitreous materials from Tolochenaz shows that they are 6 glass and 1 glass faience beads. All the glasses from the body and the decoration of the beads, such as the glass phase of the glassy faience, have LMHK composition, with chemical variation depending on the type of colour. The comparison of the data with the ones available for coeval European glasses evidence a good similarity and a particularly satisfactory correlation may be found with the materials from Hauterive NE – *Champréveyres* and those from Northern Italy.

The presence of a red annular beads represent a strong link with the Frattesina production and North Italy, whereas the glassy faience biconical bead is a clear connection with the vitreous materials from Hauterive NE – *Champréveyres*, where faience with comparable composition have been reported (Henderson 1993). Locally produced glassy faience with LMHK composition are known in Northern Italy at the beginning of the Middle Bronze Age, but to date there are no examples dated to the FBA (Angelini *et al.* 2002b, 2005a; Bellintani *et al.* 2005, 2006; Angelini 2011; Artioli, Angelini 2013). With the exception of one faience with a typical Mycenaean typology (lenticular bead, radially grooved), no faience or glassy faience beads are reported from Frattesina (Bellintani *et al.* 2006), even if the term "glassy faience" in some cases is used to describe glasses with a particularly high amount of inclusions (Santopadre, Verità 2000).

In order to fully understand the development of glass production in Bronze Age Europe, more analytical data are needed, but it is extremely important that the investigations are performed on objects with a secure archaeological context. A clear correlation of the evolution of the glass chemical recipes with the chronological phases, distinct for each specific geographic area, is still lacking. Moreover, due to the extremely heterogeneous nature of the Bronze Age glasses, beside the chemical analyses a mineralogical and textural characterization of the materials may strongly help.